University of Twente

# Modeling the heat transfer of a packed bed with an effective thermal conductivity


E.A. Haselhoff - s1120891

Internship supervisor: ir. M.J. Botman
UT supervisor: Dr. ir. A.K. Pozarlik


16th of August 2017

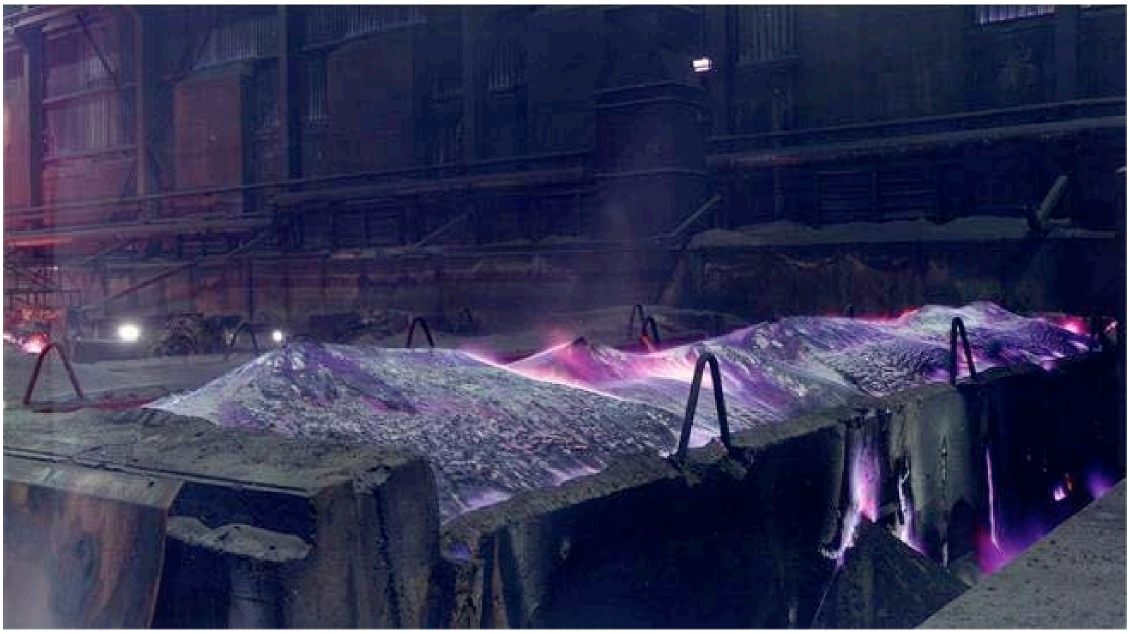

# Preface

My personal interest in thermodynamics brought me all the way to Hengelo where I discovered the small but interesting company Reden, which is a small research company offering engineering solutions on an academic level. I had the pleasure to work here from the end of February to the beginning of June, during which I had a great experience and could apply knowledge that I learned in the past years while being shown that there is always (much) more to be learned.

The small size of the company reflects in the working environment. Communication is fast, meetings are only necessary when you actually have something important to discuss, and the people are laid-back, which creates for a very pleasant working environment. On top of that it was a unique experience to see that much emphasis is laid on the importance of understanding the issue you are working on, while on the other hand finding the balance between this (fundamental) research and actually applying knowledge toward a practical solution in a relatively short amount of time.

To Maarten Botman, thanks for the engaging discussions we have had, for spotting mistakes I made and for your feedback as supervisor; these have greatly helped me in my endeavours. I want to thank everyone at Reden for the many laughs and interesting conversations I have had. If I would have to blame you for something it would be for spoiling me with your proper coffee; I will never be able to digest the university coffee any more.

Special thanks go out to Enne Faber and ESD-SiC for providing data and showing interest in this work by inviting us over in Farmsum. Being given the possibility to see the actual process and the bigger picture behind this research gives a sense of tangibility, which can easily be lost when only working on the mathematics. Additionally thanks to Arthur Pozarlik for being my university supervisor and taking the time to review the presented work.

## Abstract

This research describes the findings of an internship carried out at Reden in Hengelo, where the research goal was to gain insight on the heat transfer of a packed bed as for example used in the Acheson process where cokes and quartz sand are mixed and heated up. Literature research has been done on models concerning heat transfer through packed beds. Focus was put on mono-beds consisting of one type of particle rather than binary-beds of two types of particles, since the latter subject was deemed too complex.

Analytical models from literature were chosen to model conduction and radiation, which rely on homogenisation of the bed such that a unit cell can be defined in order to determine the effective thermal conductivity. This can be used to analytically study the influence of parameters like material, particle and bed structure properties. These models have been used to gain understanding on how heat transfer behaves for quartz sand, where it is shown that particularly the particle diameter has a strong influence on the effective thermal conductivity.

A shortcoming of these mathematical models is the reliance on a perfect structure for homogenization, hence first iterations of a FEM model have been created such that these can be further developed to research more complex cases. Further development of these models and additional validation is still needed.



**Keywords:** packed bed, effective thermal conductivity, heat transfer, radiation, conduction, FEM

# Contents

# List of Figures

# List of Tables

# 1 Nomenclature

Table 1: Symbols

| **Symbol** | **Unit** | **Meaning** |
|---|---|---|
| $a1 - a2$ | - | Empirical constants |
| $A_r$ | $m^2$ | Surface area of the unit cell |
| $A_s$ | $m^2$ | Surface area of the sphere |
| $b_L$ | $m$ | Macrogap chord |
| $c_1$ | $GPa$ | Micro-hardness coefficient |
| $c_2$ | - | Micro-hardness exponent |
| $d_p$ | $m$ | Particle diameter |
| $f_k$ | - | Non-isothermal correction factor |
| $F_{1-2}$ | - | View factor |
| $F$ | $N$ | Contact force |
| $E'$ | $GPa$ | Equivalent Youngs modulus |
| $E_{1,2}$ | $GPa$ | Youngs modulus of a particle |
| $H^{'}$ | $GPa$ | Equivalent micro-hardness |
| $H_B$ | $GPa$ | Brinell hardness |
| $H_{BGM}$ | $GPa$ | Hardness constant 3.178 GPa |
| $H_{vic}$ | $GPa$ | Vickers micro-hardness |
| $k_g$ | $\frac{W}{mK}$ | Thermal conductivity of gas phase |
| $k_s$ | $\frac{W}{mK}$ | Thermal conductivity of solid phase |
| $K_{e,r}$ | $\frac{W}{mK}$ | Effective thermal conductivity by radiation |
| $K_{r,L}$ | $\frac{W}{mK}$ | Long-range radiation conductivity |
| $K_{r,S}$ | $\frac{W}{mK}$ | Short-range radiation conductivity |
| $m_rms$ | - | Combined root mean squared surface slope |
| $M$ | $m$ | Gas parameter |
| $\bar{n}$ | - | Coordination flux number |
| $\bar{N}_c$ | - | Coordination number |
| $P_0'$ | - | dimensionless contact pressure |
| $P_{0,H}$ | $Pa$ | Hertzian contact pressure |
| $P_0$ | $Pa$ | Maximum contact pressure |
| $r_a$ | $m$ | Radius of rough contact area |
| $r_H$ | $m$ | Radius of Hertzian contact area |
| $r_p$ | $m$ | Radius of sphere |
| $R_g$ | $\frac{K}{W}$ | Resistance of the interstitial gas in the micro-gap |
| $R_G$ | $\frac{K}{W}$ | Resistance of the interstitial gas in the macro-gap, |
| $R_{hertz}$ | $\frac{K}{W}$ | Hertzian micro-contact resistance |
| $R_l$ | $\frac{K}{W}$ | Resistance of the macro-contact constriction |
| $R_s$ | $\frac{K}{W}$ | Resistance of the micro-contact |
| $T$ | $K$ | Particle surface temperature |
| $T_{avg}$ | $K$ | Bed average temperature |
| $Q_r$ | $W$ | Heat transfer by radiation |

Table 2: Greek symbols

| **Symbol** | **Unit** | **Meaning** |
|---|---|---|
| $\alpha$ | - | Non-dimensional parameter |
| $\epsilon_r$ | - | Emissivity of the particle surfaces |
| $\kappa$ | - | Non-dimensional parameter |
| $\mu_{1,2}$ | - | Poissons ratio of particle |
| $\sigma_{sb}$ | $\frac{J}{m^2 s K^4}$ | Stephan-Boltzman constant |
| $\sigma_{rms}$ | $m$ | Combined root mean squared surface slope |
| $\bar{\phi}_c$ | Degrees | Average contact angle |
| $\omega_0$ | $m$ | deformation depth |

Table 3: Abbreviations

| **Abbreviation** | **Full meaning** |
|---|---|
| ETC | Effective thermal conductivity |
| SC | Simple cubic |
| FCC | Face centered cubic |

## 2 Introduction

The production of silicon carbide (SiC) is carried out by means of the Acheson process, named after its inventor Edward Goodrich Acheson. In this process, a mixture of quartz sand and coke is heated to a maximum temperature of 3000 K through resistance heating using a graphite core through which a current is passed. After a number of reactions silicon carbide is formed with as main by-product carbon monoxide.

Production ovens based on this principle are built in an open field. First a U-shaped graphite core is created on which the mixture of quartz sand and coke is put, where after this reaction bed is covered up with a tarp to capture the reaction gases. The dimensions of such a production furnace are about 20 x 20 x 6 meters and the production process is characterized by a high energy demand. The input power of a typical production oven is 10 MW and 6 MWh is necessary for the production of 1 ton SiC. An oven journey takes about 200 hours, which produces between 300 and 370 tonnes SiC.

Figure 2.1: Production of SiC at ESD-SiC

There are several important transport mechanisms for heat transfer through the bed: conduction through the solids, conductivity through cavities, transfer via radiation and convection of the interstitial gases; these largely determine the temperature gradient between the core and the shifting reaction zone. Additionally this heat transfer is influenced by factors such as the overall temperature, the grain size distribution, impurities, and the contact pressure between the grains.

The goal of this research is to gain insight in the heat transfer properties of the bed by means of a simulation model describing the heat transfer by conduction and radiation in the packed bed. Convection has been left out due to simplicity. Chapter 3 focuses on the results of the literature research. Based on this a mathematical model of a mono-bed, having only one sized type of particle, is show in chapter 4 in which convective heat transport has been excluded. This model allows to analytically express the conduction and radiation, which can be used to gain initial understanding of the mechanisms and influence of parameters. First iterations of FEM models are shown in chapter 5 for both conduction an radiation as well, since the mathematical model relies on simplification of reality where FEM can complement for more complex cases.

# 3 Literature

## 3.1 Modelling of packed beds in literature

The initial literature study focussed on binary packed beds, in order to gain knowledge on how such a bed consisting of two different types of materials would behave. However, it became apparent that research concerning these beds have an experimental focus. Different conditions and packing possibilities due to the size ratio of the particles are still actively studied and require numerical simulations in order to gain understanding of the behaviour of such a bed.

It became apparent that this subject is quite complex and still not well understood, which would make it difficult to create an applicable model. However, much more could be found on the topic of packed mono-beds, having particles of only one size. Due to its considerable interest in applications of thermal insulation, catalytic reactors, breeder blankets for fusion reactors and other thermal systems associated with high energy transfer, more research seems to have been conducted on this topic.

Numerical models are possible by using the Discrete Elements Method (DEM) and Voronoi cells [2] for example, which allows to easily quantify the void fraction of a random bed and consider the wall region effects. They give good results for contact resistance and heat transfer, but simulations are mostly made for smaller pebble bed reactors. For large beds it becomes computational very expensive, especially if radiation is included. Furthermore, a big advantage of DEM is that it can describe the dynamics of moving particles. The packed bed in consideration will remain stationary, which means a big reason to use DEM will not be utilized.

Interest was therefore taken in a specific selection of papers with an approach to analytically model a packed bed. If the bed is considered to have a certain ideal structure it is possible to zoom in and define a unit cell. Properties of the particles can be taken into consideration and an effective heat transfer conductivity is determined on this level. The beauty of this method is that the influence of certain parameters can be considered solely on the unit cell level, but because of its homogeneous nature it can be used to describe the characteristics of the entire bed.

## 3.2 Papers with analytical homogenisation model

Slavin et al. [3] [4] [5] was one of the earlier papers found to takes into consideration the different paths of heat in a unit cell, which can be used to model the effective thermal conductivity in a packed mono-bed of solid spheroids. However, the developed model makes certain assumptions about the bed to hold true, like having a hard material with high conductivity. Furthermore Slavin uses his own simplified model of contact between the spheres containing several parameters that are fixed by fitting it to experimental data. The model is therefore only valid for specific conditions, but still presents some important conclusions. One of them is that knowledge of the roughness of the particles is critical, which apparently was not always considered in experiments and another that the resistance of the contact points is much higher than that of the surrounding gas, which would mean that the conductance in some cases could be neglected if compared with the conductance through the gas.

In his last paper [5] an attempt was made to transform the model to be used for a binary bed of two materials. The approach used is to assume that one material has a much smaller size than the other, such that it can fit between the gaps of the larger material. The conductivity of the cavities of the larger spheres is then considered to be uniform and equal to the value obtained from the mono-bed model for the tiny spheres alone. Due to the lack of published experimental data it could only be compared against one experiment. It was found to agree well, but more testing was obviously advised.

Bahrami [6] [7] worked in conjuncture with Yovanovic who deserves a honourable mention for his research that goes back to the '60. Over the years he published research on thermal contact, thermal gap, and thermal joint resistances and conductances with applications to microelectronics. His theories on thermal contact allowed amongst others Bahrami to develop his model. Bahrami et al. researched the thermal joint resistances of rough non-conforming surfaces, which was used to develop a model that could predict the effective thermal conductivity of a packed bed [1]. It argued that radiation between spheres would remain small for most applications and natural convection does not occur due to a Grashof number lower than 2500, hence the focus would purely be on heat transfer because of conduction.

The approach taken was to assume a periodic structure throughout the bed, where emphasis was placed on the simple cubic (SC) and face-center cubic (FCC) structure; see figure 3.1. They argue that since these are the least and most dense packings, respectively, they form an upper and lower bound for the effective thermal conductivity of a real randomly packed bed. The model does not account for tangential forces in the contact area, which are of influence for a FCC packing. Thus the model was shown to agree well with experimental data for SC, but is not as accurate for FCC. The trends are captured in both cases however, so the effect of important parameters can be studied by using these regular structures in order to characterise the behaviour of a randomly packed bed.

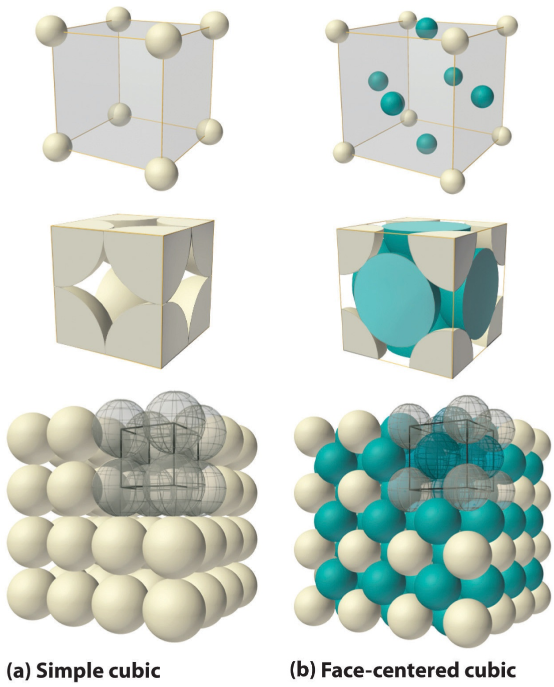


Figure 3.1: SC and FCC structure of particles

Van Antwerpen et al. provided an in-depth review of literature [8] describing the packing structure and effective thermal conductivity of randomly packed beds consisting of mono-sized particles, where attention was given to the packing structure (porosity, coordination number, and contact angles) and heat transfer by solid conduction, gas conduction, contact area, surface roughness, as well as thermal radiation. An important conclusion made was that when heat transfer in a packed bed is considered the effect of the packing structure cannot be characterized by the porosity alone, thus the coordination number and the contact angles between adjacent particles must also be

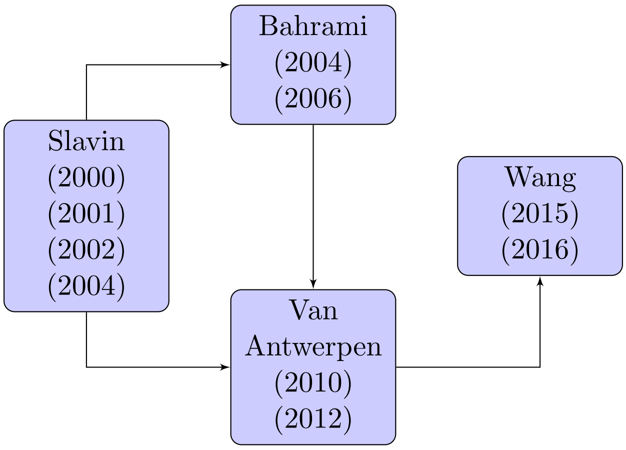


Figure 3.2: Papers and their influence on each other

considered.

From this knowledge a model was developed to determine the effective thermal conductivity containing both conduction and radiation [9]. The conduction part is similar to Bahrami et al., but more extensive by accounting for more regimes in the unit cell and additionally includes a comparison with Hertzian contact. Radiation was split up in short-range radiation between contacting particles and long-range radiation between particles that can 'see' each other through the voids of the bed.

It was argued that at higher temperatures the thermal radiation component of the effective thermal conductivity becomes dominant, but also that a variation in sphere diameter and solid conductivity has an influence on its magnitude. Furthermore, since it focusses on nuclear pebble reactors - which have a relatively small packed bed - additional equations are given to take into account the effects the walls have on the effective thermal conductivity of the bed. It is later shown this effect can be neglected if the bed is large enough.

Wang et al. [10] [11] present a model which includes a modified Bahrami conduction, a modified Van Antwerpen radiation and an additional model for convection. However, its contact model is much more simplified compared with the Bahrami/Yovanovic model, the conduction model also neglects particle roughness and its convection model needs empirically determined constants which were acquired by using FEM.

## 3.3 Selection of model

The previously mentioned papers all follow the same philosophy and do influence each other, as can be seen in figure 3.2. Even so, the models do differ from each other such that a choice had to be made which ones were deemed more suitable.

Slavin relies on assumptions to hold true about the bed and the material in order to be valid, such that it would have no changeable parameters. Wang also relies on some assumptions, which makes it loose some flexibility and bases its work on Bahrami and Van Antwerpen. There models were therefore not deemed to be the most practical.

From the remaining two papers it was chosen to focus on the conduction model of Bahrami and the radiation model of Van Antwerpen. The reason for conduction being that it is the simpler of the two and seemed a better point to start and understand the underlying mechanisms. If deemed necessary one could always make it more complex by moving to the conduction model from Van Antwerpen, hence for now only his model of radiation is used.

# 4 Mathematical Model

In literature it is stated that the effective thermal conductivity is defined by conduction through the solid and gas, radiation between the particles and convection if the particles and/or gas is in motion. Only the first two phenomena are considered since the interstitial gas is assumed to remain stagnant. They are modeled separately to determine the conductivity of that specific part, which together express a total effective thermal conductivity of the unit cell [1] [9]:

$$k_{eff} = k_c + k_r \tag{1}$$

In the next sections the mathematical model for conduction and radiation is explained in more detail. The conduction part is a simplified overview to maintain readability; the complete set of equations can be viewed in appendix A, which includes references to their paper of origin. The symbols as defined by Van Antwerpen [9] have been used for both conduction and radiation, since its nomenclature was more detailed than the one provided by Bahrami et al. [1].

The complete model has initially been created in Matlab since it personally allowed for quicker and easier prototyping, but has later been recoded to the more generally usable Python. Results shown in sections 4.3 and 4.4 have been generated by using Matlab.

## 4.1 Conduction

### 4.1.1 Unit cell

The basic idea of this model is to assume that the packed bed in consideration has a periodic structure. This allows to define a smallest usable scale - a unit cell - that can be homogeneously applied to the entire bed. See figure 4.1.

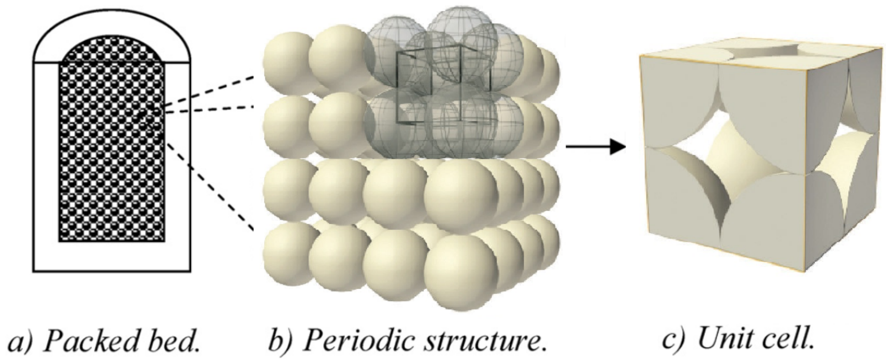


Figure 4.1: Schematic of homogenisation method of the unit cell

As mentioned before, the FCC and SC packing are the most dense and least dense, respectively, so they they can be used as an upper and lower bound for the effective thermal conductivity of a random packed bed; for this reason Bahrami et al. [1] used these two packings. Single parameters, like the sphere roughness or particle diameter, can be changed and its effect on the unit cell can be calculated. This offers the possibility to study the behaviour of a randomly packed bed. For now only the SC structure is modelled, since it is the most simple of the two and is used to make the initial step. Other packing structures can always be included in future versions using the same unit cell approach.

### 4.1.2 Joint thermal resistance

The present model looks at the different conduction paths in a unit cell, which are illustrated in figure 4.2a, each expressed as a thermal resistance. There are two main paths: through the macro air gap between the particles, which has a resistance $R_G$, or through the contact area between the spheres. Heat going through the solid particle will eventually be constricted when passing the area of contact, which is defined as the macro-contact resistance $R_L$. In this macro-contact area between the spheres heat can either conduct through micro-contacts with resistance $R_s$ or pass through the micro-gaps around the micro-contacts, which has a resistance $R_g$. These different paths can be represented as a thermal resistance network from which a joint thermal resistance can be calculated. See figure 4.2b. The unit cell can now be characterised as if it were of a homogeneous material with the same thermal resistance.

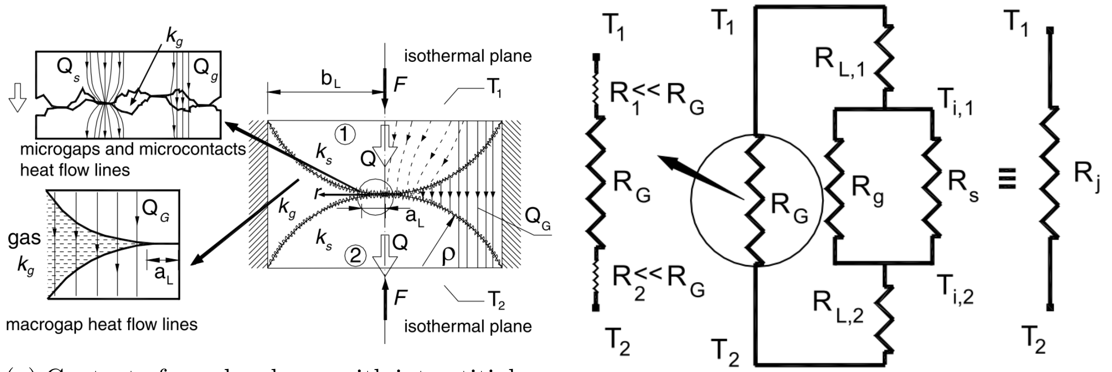


(a) Contact of rough spheres with interstitial gas

(b) Thermal resistance network

Figure 4.2: Conduction modeling between two spheres

The total joint thermal resistance can be calculated by:

$$R_j = \left[ \frac{1}{\left(\frac{1}{R_s} + \frac{1}{R_g}\right)^{-1} + R_L} + \frac{1}{R_G} \right]^{-1} \tag{2}$$

### 4.1.3 The different thermal resistances

An overview of the different thermal resistances is given and briefly shows the mathematics behind them. In the appendix A.4 the formulas and their references to literature can be found in more detail.

The model assumes that the particles are randomly rough in which the contact between these two Gaussian rough surfaces is modeled by a perfectly smooth surface and a single Gaussian surface with combined properties of both particles. Its thermal resistance is determined by:

$$R_s = \frac{0.565}{k_s F} \frac{\sigma_{rms}}{m_{rms}} \tag{3}$$

No mention is made by Bahrami et al. [1] of the used values for the slope $m_{rms}$, but it is very likely a correlation proposed by Lambert and Fletcher is used as shown by Bahrami in a previous paper [7]. It was found using experimental results of different types of stainless steel and determined to have a 15% accuracy bound for other metals.

Furthermore, the heat passing through the sphere will encounter the constriction caused by the macro-gap, also called the spreading resistance:

$$R_L = \frac{0.5}{k_s r_a} \tag{4}$$

Bahrami et al. developed an analytical model to predict the heat conduction through a stagnant interstitial gas between rough spherical bodies [1]. It accounts for all regimes of gas heat transfer, which are conduction modes from continuum to free molecular. The region between the solids is divided into infinitesimal surface areas, where the total resistance is determined by integrating over the total area. This results in expressions for the micro-gap $R_g$ and macro-gap $R_G$ resistances [6]:

$$R_g = \frac{2\sqrt{2}\sigma_{rms}a_2}{\pi k_g r_a^2 \ln\left(1 + \frac{a_2}{a_1 + \frac{M}{2\sqrt{2}\sigma_{rms}}}\right)} \tag{5}$$

$$R_G = \frac{2}{\pi k_g \left[S \ln\left(\frac{S-B}{S-A} + B - A\right)\right]} \tag{6}$$

where $a_1$, $a_1$, A, B and S depend on sphere and contact dimensions.

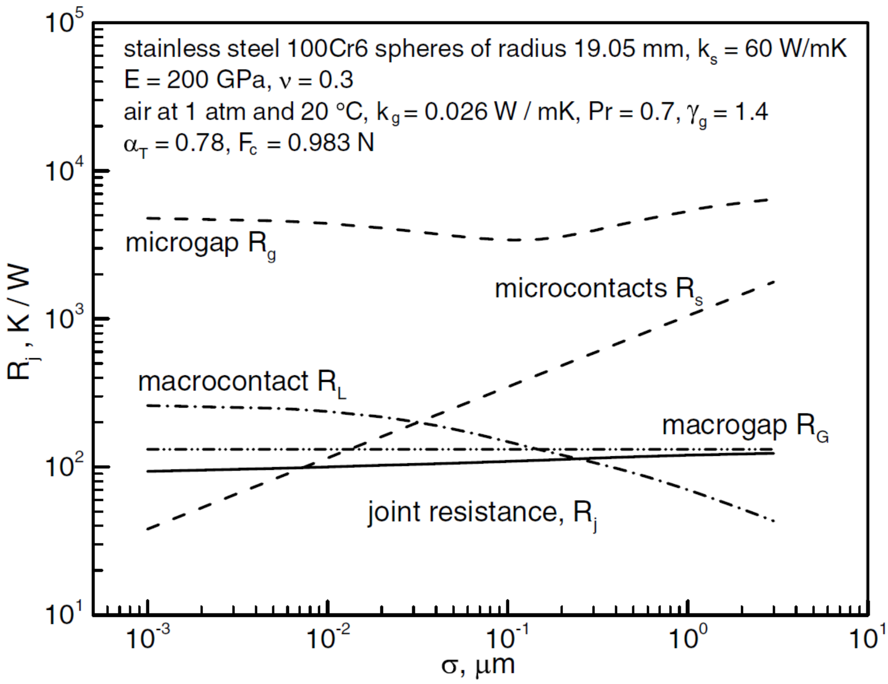


Figure 4.3: Effect of roughness on the resistances as given by Bahrami et al. [1].

Figure 4.3 shows the influence of roughness on a SC packing with parameter values as seen in the figure itself. These correspond to a test-bed as presented by Bahrami et al. [1] in order to validate the model with experimental data. In this case the roughness is increased while the other listed parameters are held constant. It can be seen that with higher roughness the micro-constant resistance $R_s$ (3) will increase exponentially. The reason for it not being first order has to do with the dependency on the slope $m_{rms}$, which is determined for every specific value of roughness.

Next, imagine having two perfect spheres that touch at a single point only. Increasing the roughness will result in more points of contact, which will increase the total contact area, here defined as the macro-contact area. Since this contact area becomes larger, the macro-contact resistance $R_L$ (4) will start to decrease. As a direct result of the increasing macro-contact the macro-gap area must decrease; $R_G$ (6) will therefore increase, but as can be seen the effect is barely noticeable. The reason for this is that the area of the macro-contact is very small in comparison with the macro-gap area of the gas. Even if the contact area becomes twice as large, the gas area remains approximately the same.

Lastly the micro-gap gas resistance $R_g$ (5) shows an interesting behaviour. With decreasing roughness, the air pockets between the roughness peaks will start to decrease. As a result the resistance will also become lower, until it hits a lowest point. Decreasing the roughness even further will actually have the opposite effect. This has to do with the gaps becoming smaller than the mean free path of the air molecules and the rarefaction effect of the gas being taken into account. It becomes easier for the air molecules to exit the gaps than to stay in them, effectively lowering the amount of molecules and thus air pressure. As result it increases the resistance.

### 4.1.4 Effective thermal conductivity of a unit cell

In the model, the axial load is assumed to be an average value and constant throughout the bed, which is justified by explaining that the load due to total weight of the particles will linearly increase with a higher bed [1]. This average load is thus taken as the mean between the highest and lowest contact load, resulting in half the weight of the total bed. While this allows for easier homogenisation, it should be taken into account that in reality the contact load is a function of the height, which will influence the temperature field in the bed; this is important since both the materials conductivity and amount of radiation is dependent on temperature.

This unit cell is assumed to conduct heat in one dimension; the top, bottom and the macro-contact region are therefore assumed to be isothermal and the lateral sides are adiabatic due to symmetry [1]. The effective thermal conductivity of a unit cell can be found by assuming a homogeneous medium with the same resistance as the joint thermal resistance $R_j$ as shown in equation (2):

$$k_c = \frac{L_c}{R_j A_c} \tag{7}$$

where $L_c$ is the length in $m$ of the unit cell and $A_c$ the surface area in $m^2$ the heat goes through.

Bahrami et al. [1] include the boundary resistance $R_{BC}$ which arises due to imperfect contact between the bed and the wall with which thermal energy is exchanged. The effective thermal conductivity of the bed can then be calculated from:

$$k_{c,bed} = \frac{L_{bed}}{A_c(R_{bed} + R_{BC})} \tag{8}$$

$$R_{bed} = \frac{L_{bed}}{k_c A_c} \tag{9}$$

When the size of the packed bed is much larger than the size of your particle, it is possible to neglect this boundary resistance. For $L_{bed} = nL_c$, where n is the number of stacked unit cells, this can be shown as:

$$k_{c,bed} = \frac{L_{bed}}{A_c(R_{bed} + R_{BC})} \tag{10}$$

$$= \frac{L_{bed}}{\frac{L_{bed}}{k_c} + A_c R_{BC}} \tag{11}$$

$$= \frac{nL_c}{\frac{nL_c}{k_c} + A_c R_{BC}} \tag{12}$$

$$= \frac{n}{n + \frac{A_c k_c}{L_c} R_{BC}} k_c \tag{13}$$

$$= \frac{n}{n + \frac{R_{BC}}{R_j}} k_c \tag{14}$$

So for $n \gg \frac{R_{BC}}{R_j}$ the boundary resistance can be neglected, which for large packed beds will always be the case. Additionally in literature it is mentioned that this will hold true if the ratio between the bed and particle diameter is more than $\frac{L_{bed}}{d_p} = 50$ [1]. Both methods can be used to estimate if this simplification can be made.

In case of the SC structure the effective thermal conductivity can thus be found by:

$$k_c = \frac{L_c}{R_j A_c} \tag{15}$$

$$= \frac{d_p}{R_{j,SC} d_p^2} \tag{16}$$

$$= \frac{1}{R_{j,SC} d_p} \tag{17}$$

As for the SC arrangement, the effect of frictional/tangential forces is small and therefore neglected in the model. [1]. The FCC model is also worked out, but the assumption has been made to neglect tangential forces even though the spheres are stacked diagonally in the unit cell. In the paper of Bahrami et al. it is mentioned that a quantitative comparison can not be made, since as expected the difference between the data and the model show more deviation for higher values of roughness. A qualitatively comparison of the trend can be made however [1].

Using the thermal joint resistance $R_j$ as shown figure 4.3 and equation (17), the effective thermal conductivity $K_e$ for the SC unit cell can be calculated. The model is compared in the paper against experimental data points, which can be seen in figure 4.4, and is used to conclude a good agreement between them.

## 4.2 Radiation

Heat transfer by radiation will play a significant part at higher temperatures.

Solely considering the previously defined unit cell is not sufficient in this case, since besides from radiation inside the unit cell, there is also radiative transport between close neighbours in contact and even a contribution of particles at longer distance through the gaps in the bed. The model therefore defines two components: short range $K_{r,S}$, which accounts for exchange between spheres in contact, and long range $K_{r,L}$, which takes the radiation through the voids into consideration. Together they express the effective thermal conductivity by radiation [9]:

$$k_r = k_{r,S} + k_{r,L} \tag{18}$$

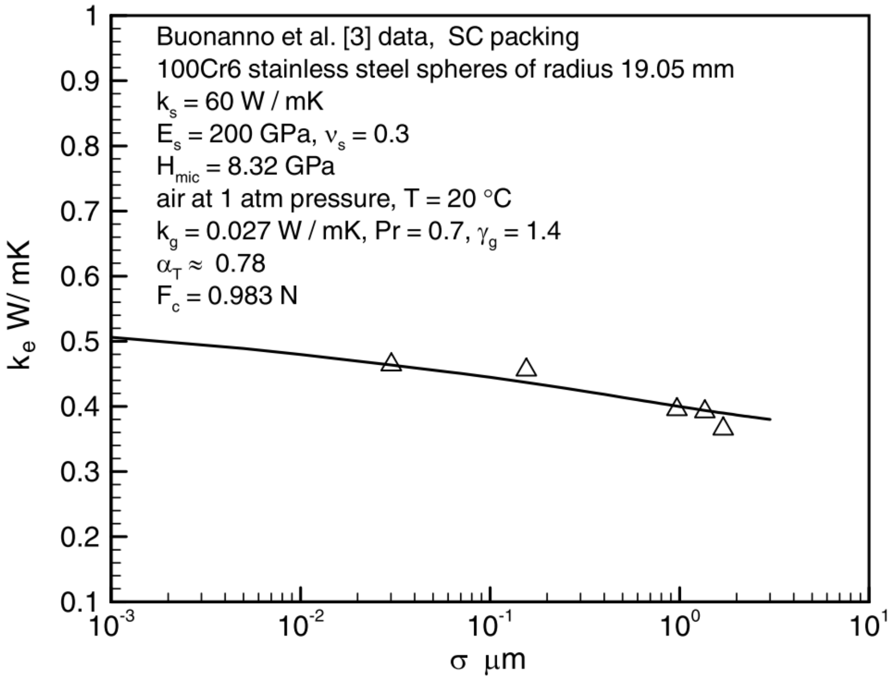


Figure 4.4: Validation with experimental data of the ETC as function of the particle rougness [1].

### 4.2.1 Short-range thermal radiation

As explained by Van Antwerpen et al. [9] the derivation for the short-range component is based on the assumption that two spheres in contact are approximated by two grey diffuse parallel plates of the same emissivity $\epsilon_r$ and similar surface area $A_s$ as the spheres. The radiation heat transfer is found from:

$$Q_r = \frac{A_s \sigma_{sb}(T_1^4 - T_2^4)}{\frac{(2-2\epsilon_r)}{\epsilon_r} + \frac{1}{F_{1-2}}} \quad \text{(VA 48)} \tag{19}$$

where the Stephan-Boltzmann constant $\sigma_{sb} = 5.67e^{-8}\frac{W}{m^2K^4}$, $A_s = 4\pi r_p^2$, the view factor is given to be $F_{1-2} = 0.0756$ and $T$ the temperature in Kelvin on one of the surfaces. Using the same $L$ and $A$ as chosen for the conduction in equation (7) the effective radiative conductivity can therefore be calculated to be:

$$k_{r,S} = \frac{Q_r L_r}{A_r(T_1 - T_2)} \quad \text{(VA 49)} \tag{20}$$

Since the difference in surface temperature between the spheres will be small it holds that $\frac{\Delta T}{T_{avg}} \ll 1$, when T is in Kelvin, which allows for the following approximation to be made:

$$\frac{(T_1^4 - T_2^4)}{(T_1 - T_2)} \approx 4T_{avg}^3 \tag{21}$$

This shows that the effective radiative conductivity is strongly dependent on the overall temperature as well as the temperature difference between two particles, where a cubic behaviour is expected.

To account for the contacting neighbours and the structure of the bed, Van Antwerpen et al. multiply with the average coordination flux number $\bar{n} = \frac{\bar{N}_c}{2}$ and average contact angle $\bar{\phi}_c$. Additionally it is mentioned that the effective radiant conductivity is strongly influenced by the thermal conductivity $k_s$ of the particles, such that the isothermal surface temperature assumption can not be made, as was the case with conduction, for lower values of $k_s$ [9]. A non-isothermal correction factor $f_k$ was therefore introduced.

Substituting equation (19) in equation (20), applying the approximation from 21 together with the above mentioned additions, this gives the following expression for short range conductivity:

$$k_{r,S} = \frac{2\bar{N}_c d_p \sigma_{sb} A_s T_{avg}^3}{A_r \frac{(2-2\epsilon_r)}{\epsilon_r} + \frac{1}{F_{1-2}}} f_k \sin(\bar{\phi}_c) \quad \text{(VA 51)} \tag{22}$$

### 4.2.2 Long-range thermal radiation

Long-range radiation is defined as thermal exchange through the voids of the packed bed by spheres that are not in direct contact with each other. In order to tackle this complex phenomenon, Van Antwerpen et al. looked at what effect the distance has to the radiative contribution; this result can be seen in figure 4.5.

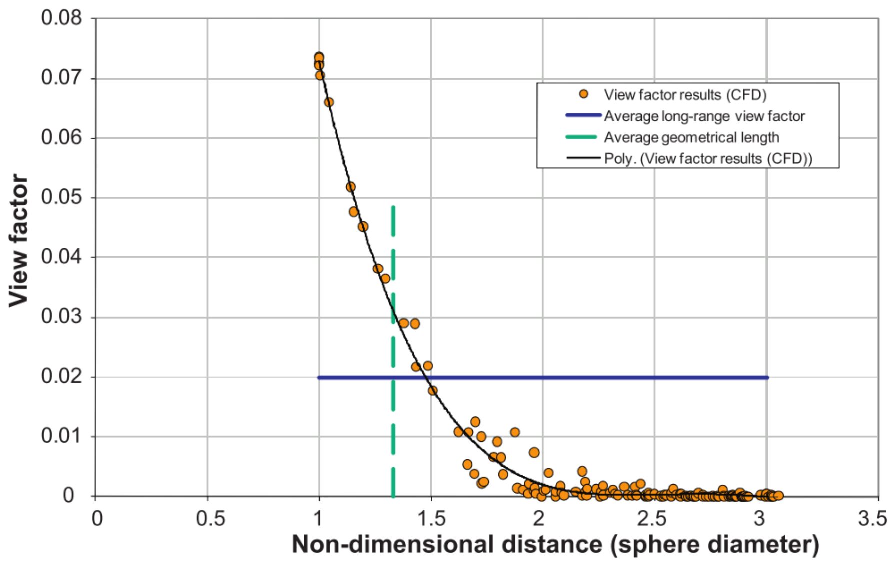


Figure 4.5: View factor as function of non-dimensional sphere distance [9].

It was noticed that after approximately 2.25 sphere diameters the view factor goes to zero. From this an average long-range diffuse view factor $F_{1-2,avg} = 0.0199$ and an average geometrical length $z_{avg} = 1.33$ were obtained, which are used to characterise the conductivity of the long-term radiation:

$$k_{r,L} = \frac{4(1.33 d_p) \sigma_{sb} A_s T_{avg}^3}{A_r \frac{(2-2\epsilon_r)}{\epsilon_r} + \frac{1}{F_{1-2}}} \quad \text{(VA 55)} \tag{23}$$

The same particle values and non-isothermal correction factor are used for the long-term radiation, however in order to account for the multiple spheres taking part a long-range coordination flux number $n_{long}$ is used instead:

$$k_{r,L} = \frac{5.32 d_p \sigma_{sb} A_s T_{avg}^3 n_{long}}{A_r \frac{(2-2\epsilon_r)}{\epsilon_r} + \frac{1}{F_{1-2}}} f_k \quad \text{(VA 56)} \tag{24}$$

Unfortunately $n_{long}$ has to be determined empirically by finding a best fit if compared to experimental data.

### 4.2.3 Thermal conductivity by radiation

As described in equation 18 the short- and long-range components contribute to the total effective thermal conductivity due to radiation. Van Antwerpen et al. [9] compared their radiation model against experimental data as can be seen in figure 4.6. The experimental data was acquired from a cylindrical vessel containing a randomly packed bed of particles of 0.04 $m$ with properties as given in the figure.

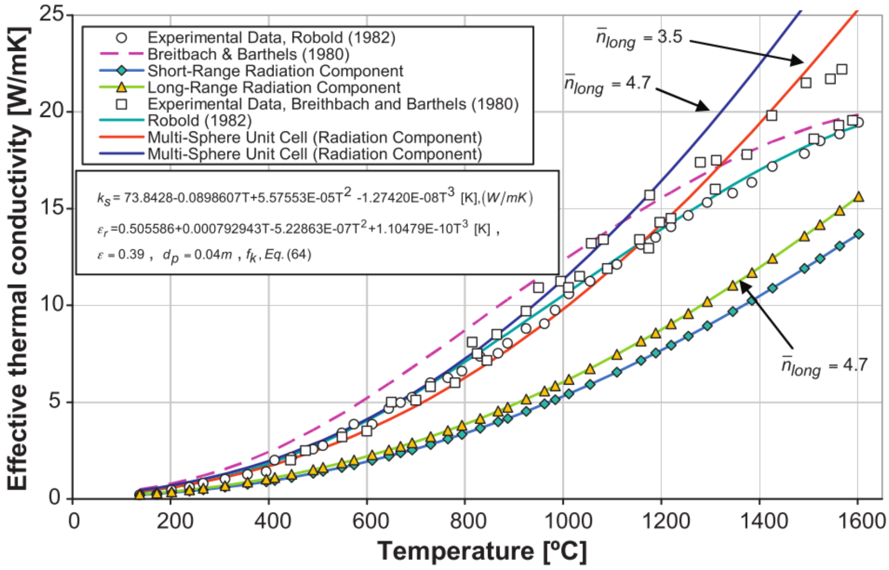


Figure 4.6: Radiation model comparison in literature with experimental data [9].

It was concluded by van Antwerpen et al. that the model best represents the experimental data when $3.5 \leq \bar{n}_{long} \leq 4.7$ and shows accuracy below $1200°C$. Van Antwerpen et al. mention that this deviation at higher temperatures might be caused by certain assumptions that where made in the model. For example, the average temperature and the non-isothermal correction factor for long-range pebbles is kept the same as short-range, while in reality this is not the case and will results in a sharper decline of $f_k$ and thus $k_{r,L}$ at higher temperature [9]. This is mentioned as a point of improvement.

## 4.3 Validation

Using the theory mentioned in the paper of Bahrami et al. [1] and Van Antwerpen et al. [9] a complete mathematical model was reconstructed for conduction and radiation, respectively. Unfortunately sometimes specific values that were used are not presented or lack better explanation, resulting in that the mathematical model can not be verified to be exactly the same as used by Bahrami and Van Antwerpen. In general small deviations in absolute values are therefore witnessed, but the trends do correspond with each other. This means that the influence of parameters can still be used to characterise the behaviour of the modelled material.

### 4.3.1 Conduction

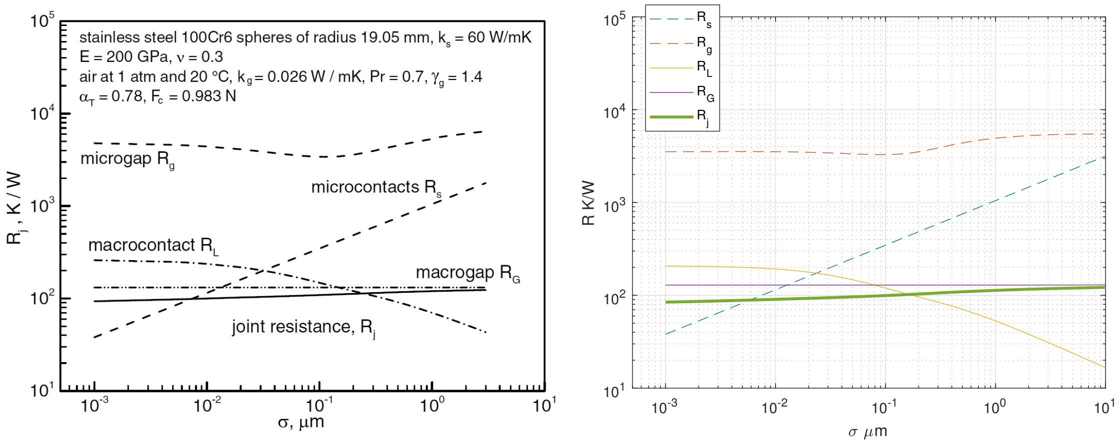


(a) SC resistances as function of sigma [1]

(b) Matlab SC resistances as function of sigma

Figure 4.7: Comparison of the thermal resistances between literature and reconstructed model

Taking a look at figure 4.7 it can be seen that the microcontact resistance $R_s$ and the macrocap resistance $R_G$ match very well. $R_g$ however shows some lower values at smaller values for roughness. As mentioned before, this region is a.o. depended on the mean-free path which is not mentioned in literature, hence a different value compared with Bahrami could explain this. Nevertheless, the general shape of $R_g$ does correspond and its influence on the total joint resistance is small. The macrocontact resistance $R_L$ is also too low for smaller roughness, which might indicate the contact area radius $r_a$ is a bit larger than it should be, but seems to correspond well for higher values. The total joint resistance $R_j$ shows the same trend, albeit slightly higher than in literature.

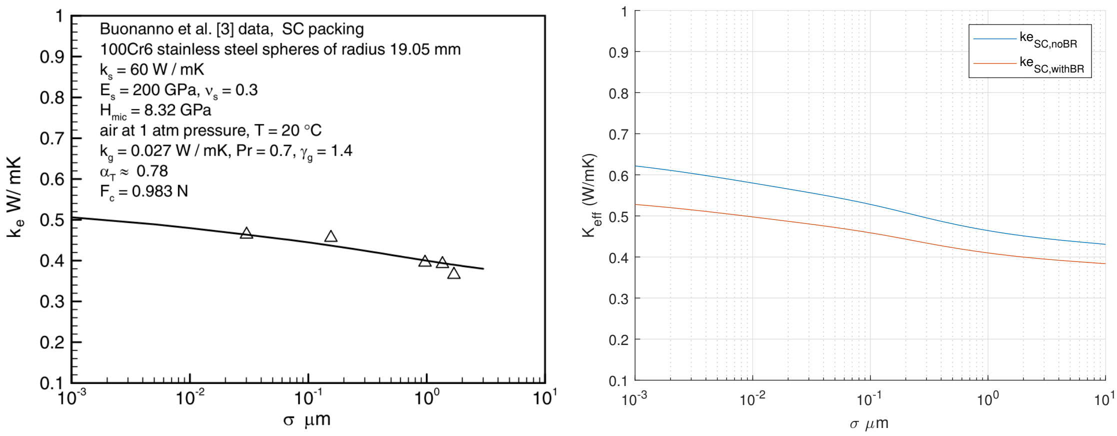


(a) Model comparison in literature and experimental data [1]

(b) ETC with and without taking the boundary resistance into account.

Figure 4.8: Comparison of the ETC using literature and reconstructed model.

The effective thermal conductivity resulting from this joint resistance is also compared. As shown in equation (8) it is possible to include the resistance with a boundary wall, however no mention of its magnitude was made. Therefore, in figure 4.8 two results are shown; one without this additional boundary resistance and one with an arbitrarily chosen value to fit the results from literature. The latter can not be used to draw any quantitative results, but the trend does show an overestimate of the effective thermal conductivity at lower values of roughness. As previously stated, this could be caused by slightly larger values for the contact area radius $r_a$, which decreases the total joint resistance. Overall the trend of the lines does correspond and as shown in equation (14) the boundary resistance can be neglected for large packed beds anyhow.

The thermal conductivity of the particles as well of the gas is taken to be constant, but no mention is made on the effect of this assumption. The following two equations have been used to find the conductivity as function of temperature for the particle and the air, where the particle corresponds with figure 4.6:

$$k_s = 73.8428 - 0.0898607T + 5.57553E^{-5}T^2 - 1.27420E^{-8}T^3 \tag{25}$$
$$k_g = 1.5207E^{-11}T^3 - 4.8574E^{-8}T^2 + 1.0184E^{-4}T - 0.00039333 \tag{26}$$

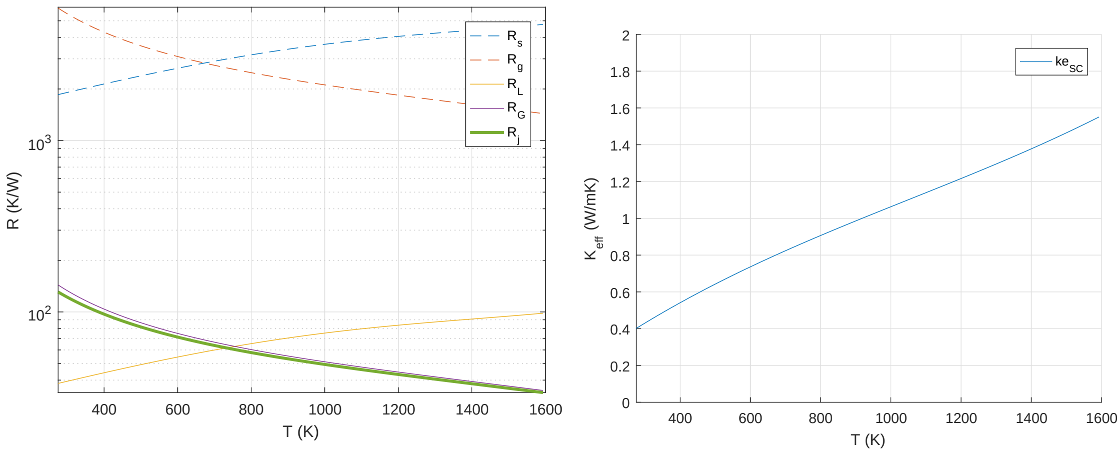


(a) SC resistances for materials with conductivity as function of temperature

(b) Matlab SC resistances as function of sigma

Figure 4.9: ETC for materials with conductivity as function of temperature.

In this case $k_s$ will decrease with higher temperature and $k_g$ will decrease. From equation (3) and (4) it can be seen that both will increase and similarly from equations (5) and (6) that they will decrease if the temperature rises. Looking at figure 4.9 it becomes obvious that the temperature will have an influence on the effective thermal conductivity. However, the radiation as seen in figure 4.6 shows a much stronger influence on temperature, hence if compared to conduction the latter would be negligible. A constant assumption for the thermal conductivities of the particles and gas therefore seems reasonable.

### 4.3.2 Radiation

Comparing the radiation result from the reconstructed mathematical model deemed difficult, since the results initially did not match for the same input parameters. Eventually it was possible to obtain the result as seen in figure 4.10b, which matches with the data as given in literature. Possibly an error was made in the paper, since the same error had to be made to create figure 4.10b. The authors also mention they expected the short-range contribution to be higher than the long-range, which is the initially obtained result; shown in figure 4.10c. In order to have a corresponding effective radiative conductivity $k_r$ the average coordination flux number is set to $\bar{n}_{long} = 1$. Although this result is in correspondence with the authors' view, a flux number of one seems too low and additionally there was no way to verify if the components have the right magnitude. However, the resulting conductivity $K_r$ is the same and the trend corresponds

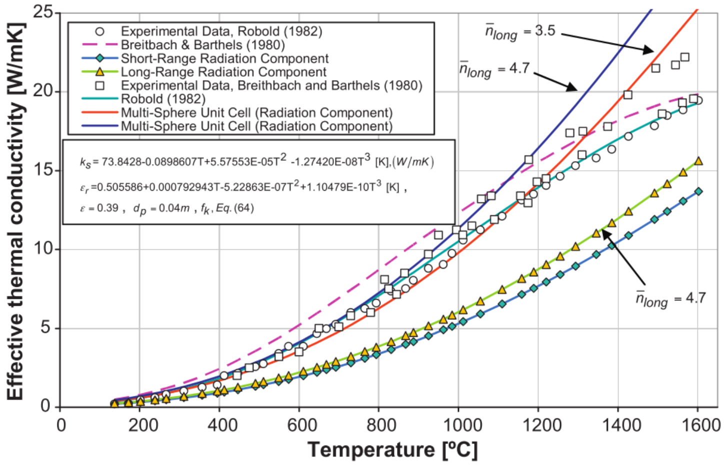


(a) Radiation model comparison in literature [9]

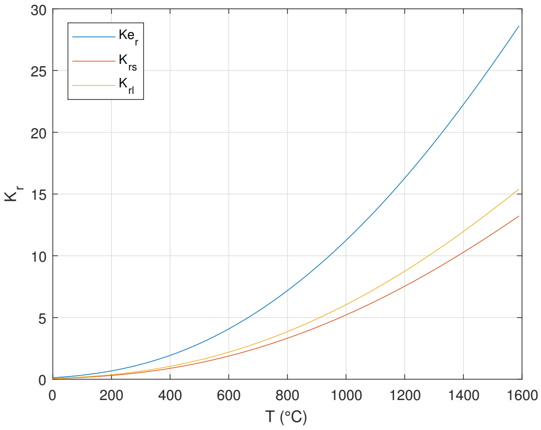


(b) Identical result - $n_{long} = 4.7$

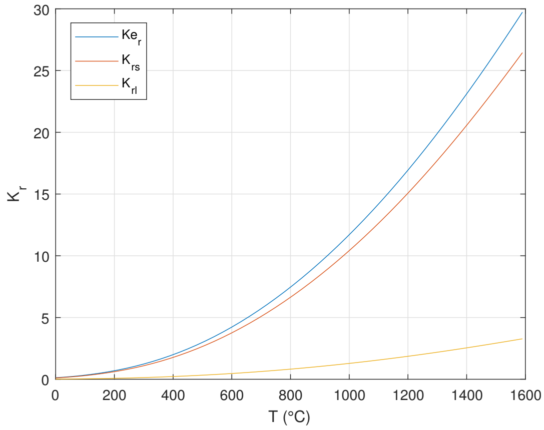


(c) Possible correct result - $n_{long} = 1$

Figure 4.10: Comparison of the thermal effective conductivity between paper and reconstructed model.

to literature, hence the results can still be used to determine the characteristic behaviour.

### 4.3.3 On Hertzian contact

While Bahrami only mentions rough contact, Van Antwerpen et al. [9] also included Hertzian contact in their paper to compare the behaviour. During this research a few funny and paradoxical results came to light that sparked interesting discussions about their validity. They will briefly be mentioned here, but serve mostly as reminder that it is important to always think what your results show, what they mean and if it is indeed what you expected.

Van Antwerpen shows the following modification to equation (2), such that in case of Hertzian contact the thermal joint resistance in the macro-contact area is expressed as:

$$R_{j,H} = \left[\frac{1}{R_{HERTZ} + R_L} + \frac{1}{R_G}\right]^{-1} \tag{27}$$

$$R_{HERTZ} = \frac{0.64}{k_s r_c} \tag{28}$$

$$R_L = \frac{0.5}{k_s r_c} \tag{29}$$

where from Hertzian contact mechanics was shown that the radius of the macro-contact is found by:

$$r_c = \left(\frac{3}{4}\frac{F r_p}{E_p}\right)^{\frac{1}{3}} \tag{30}$$

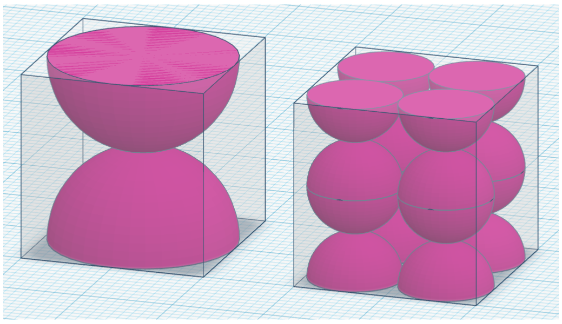

Figure 4.11: Fixed box filled with two sizes of unit cells.

A look is taken a fixed box in which we can place exactly one unit cell, see the left of figure 4.11. Lets assume unity for the particle radius, the force and Young's modulus; this box will only have one contact area in the middle:

$$r_{c1} = \left(\frac{3}{4}\frac{1 1}{1}\right)^{\frac{1}{3}} \approx 0.91 \tag{31}$$

$$A_{c1} = \pi r_{c1}^2 \approx 2.6 \tag{32}$$

If the radius becomes twice as small it is now possible fit eight unit cells in the fixed box; as shown on the right side, the box now has four contact areas on two different planes. The contact load will therefore be spread over four areas, so for one of these smaller contact areas the following holds true:

$$r_{c2} = \left(\frac{3}{4}\frac{\frac{1}{4}\frac{1}{2}}{1}\right)^{\frac{1}{3}} \approx 0.45 = \frac{1}{2} r_{c1} \tag{33}$$

$$A_{c2} = \pi r_{c2}^2 \approx 0.64 = \frac{1}{4} A_{c1} \tag{34}$$

It can be seen that if the radius of the sphere becomes twice as small, so will the radius of the contact area. The contact area will therefore become four times as small, but the box now has four contact areas in the same plane. Hence the total area over which the load will act will also remain the same; apparently changing size does not matter for the box in this regard.

Nevertheless, there are now two layers where constriction takes place instead of one, which intuitively seems to make heat transfer more difficult. For now, let's ignore resistance $R_G$ and choose $k_s = 1.14$, such that the contact conductance of a contact area can conveniently be determined to be:

$$
\begin{aligned}
H_c &= \frac{1}{A_c(R_{HERTZ} + R_L)} && (35)\\
&= \frac{1}{A_c(\frac{0.64}{1.04 r_c} + \frac{0.5}{1.04 r_c})} && (36)\\
&= \frac{r_c}{A_c} && (37)
\end{aligned}
$$

From this it can be seen that going from $r_{c1}$ to $r_{c2}$ the following happens:

$$H_{c1} = \frac{r_{c1}}{A_{c1}} \tag{38}$$

$$
\begin{aligned}
H_{c2} &= \frac{r_{c2}}{A_{c2}} && (39)\\
&= \frac{\frac{1}{2} r_{c1}}{\frac{1}{4} A_{c1}} && (40)\\
&= 2H_{c1} && (41)
\end{aligned}
$$

The conductance apparently becomes twice as high for the smaller contact area. Therefore, even if there is a doubling of constrictions it will cancel out with the increased conductance and as result the thermal conductivity of the fixed box will remain unaffected.

This paradoxical result that size does not matter nevertheless seems to go against intuition, since it would seem that if you go from a situation where you only have one restriction to a situation where there are multiple, the resistance encountered by the heat flow would increase. It could either be that since Hertzian contact is a perfect assumption it will therefore not resemble reality, or perhaps there is more to be understood on the matter. Whatever the case, it would be wise to further research this topic since the contact between the spheres is an integral part of the thermal model.

## 4.4 Parametric influence on quartz sand

By courtesy of ESD-SiC some sieve data of their materials was sent, amongst others containing a distribution of the grain size of the quartz sand that is used in their process. From their data an average grain size of 160 $\mu m$ has been determined, which is used as input for the model to calculate the properties of the packed bed. The other parameters are based on values found for quartz/silica sand and are given in table 4.

A look can now be taken at the thermal resistances and the subsequent effective thermal conductivity, which is done as function of the particle roughness, contact load and particle diameter.

### 4.4.1 Conduction

$R_G$ shows a much more noticeable change compared to the steel balls as shown in figure 4.7. This is amongst other caused by the differently sized macro-contact area that is formed. In case of steel balls the ratio of the macro-contact area and the particle diameter

Table 4: Used fixed parameters for Quartz sand

| **Parameter** | **Value** | **Unit** |
|---|---|---|
| $d_p$ | $1.6e-4$ | $m$ |
| $\sigma$ | $0.5e-6$ | $m$ |
| $H_{mic}$ | 11e9 | $Pa$ |
| $E$ | 30e9 | $Pa$ |
| $\mu$ | 0.3 | - |
| $M_s$ | 60.08430 | $\frac{g}{mol}$ |
| $k_s$ | 0.33 | $\frac{W}{mK}$ |
| $e_r$ | 0.7 | - |

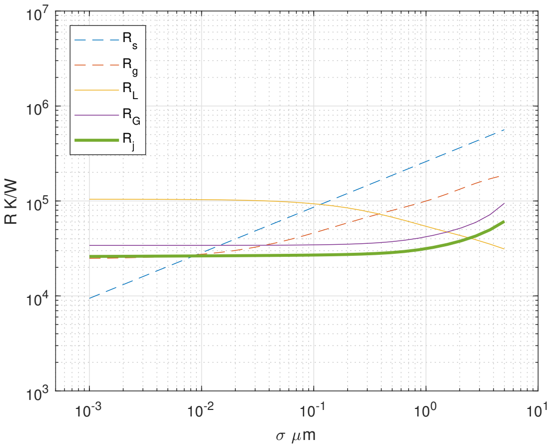


(a) Thermal resistances

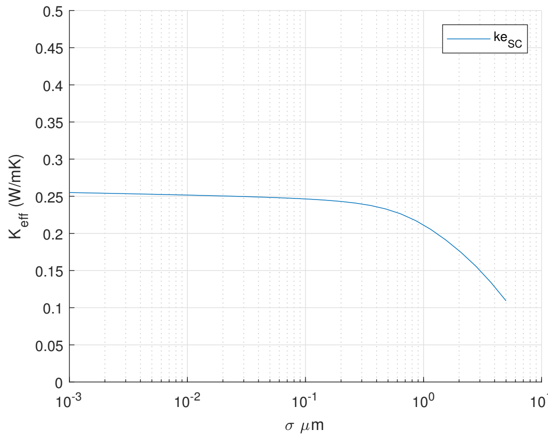


(b) Effective thermal conductivity

Figure 4.12: Influence of roughness on quartz sand SC unit cell.

would range from 0.4-5%, but with the lower Young modulus of sand and the smaller sized particle it is around 20-65%. The original argument that an increase of the macro-contact area is barely noticeable for the macro-gap is not valid any more, hence for larger values of roughness it will indeed increase. Both $R_s$ and $R_L$ still show similar behaviour, $R_s$ increasing with more roughness, while $R_L$ decreases since the macro-contact area will get larger. The rarefaction effect of $R_g$ at lower roughness values is now not as visible. It does not seem to experience a lowest point where after it increases, but simply tends to a certain limit. The latter was also the case with the larger steel balls, however it is advised to do more research on the correctness of this behaviour.

The resulting effective thermal conductivity can be seen in figure 4.12b. For higher values of roughness it was seen that the joint resistance would increase, hence the conductivity will decrease. Yet one could say that below a certain roughness, here around $0.5\mu m$, the effective thermal conductivity is independent of the surface roughness. If looking back at chapter 4.3, the values for lower roughness were overestimated, which will most likely be the case here too.

When the load on the bed and thus the contact force increases, the two spheres of the unit cell will be pressed harder against each other. This will result in a better contact with smaller micro air gaps, as can be seen in figure 4.14 by the decrease of both the microcontact $R_s$ and the microgap resistance $R_g$. This is accompanied by an increase of the macro-contact area, which in turn reduces resistance $R_L$. Again the macro-gap area will become smaller, albeit less drastically compared to the situation as seen in figure 4.12a, enlarging the macro-gap resistance $R_G$ at higher loads. Overall the effective thermal conductivity will increase, but over the several order of magnitude

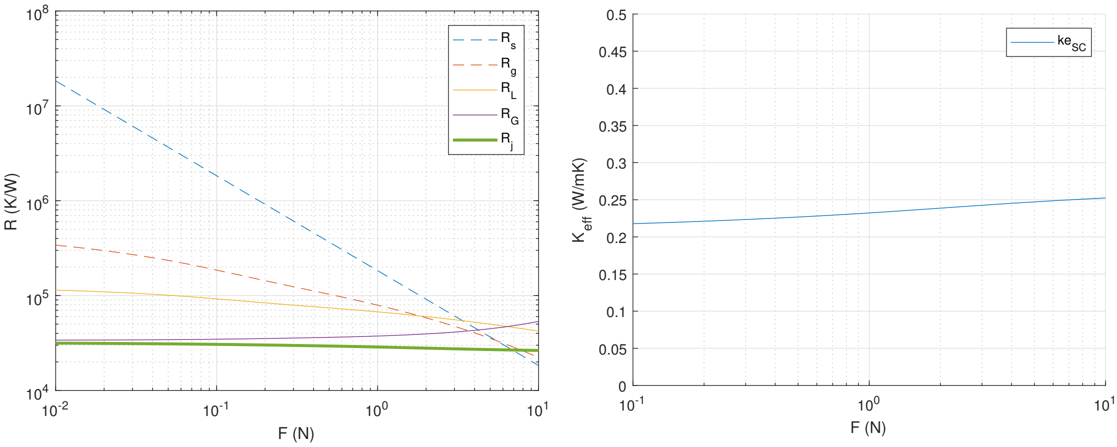


(a) Thermal resistances (b) Effective thermal conductivity

Figure 4.13: Influence of the contact load on quartz sand SC unit cell.

shown on the x-axis of figure 4.14b this change is only 15%. According to literature the validity of this result should be in good agreement with experimental data for the entire range [1].

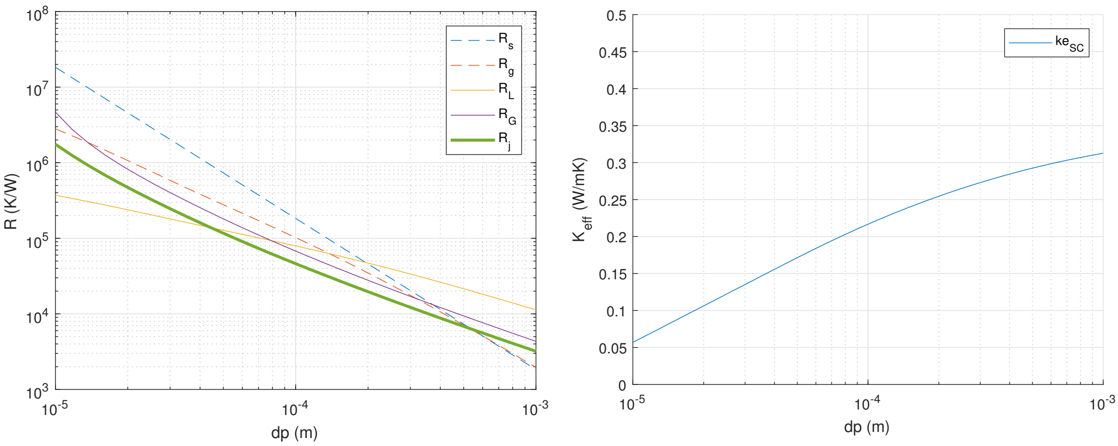


(a) Thermal resistances (b) Effective thermal conductivity

Figure 4.14: Influence of the particle size on quartz sand SC unit cell.

Lastly a look it taken at the influence of the diameter of the particles on the effective thermal conductivity. A thing to keep in mind here is that the load is assumed to remain constant for the bed and not for the unit cell. Take a look at figure 4.11; if the load on the fixed box remains the same, it has to become a quarter for each unit cell in the right case. If the load of the unit cell would remain the same it would mean that the total load on the bed would magically increase if the particles decrease in size, which does not make any sense. The contact force has therefore been scaled to the particle diameter in figure 4.14, such that the results can actually be compared with each other.

As a result the contact force between the spheres in a unit cell will decrease as the particle radius becomes smaller, hence the particles will be pressed less hard against each other. This results in worse contact of the surfaces and also larger micro-gaps in the macro-contact area, which increases $R_s$ and $R_g$ respectively. Additionally, a smaller particle also has a smaller macro-contact area, which explains why $R_l$ increases for decreasing particle size.

The macro-gap resistance $R_G$ shows an interesting behaviour, because you could expect that since the unit cell decreases in size so does the macro-gas cavity and thus the resistance would decrease. The opposite behaviour is seen, though, which is caused because the reduction of the contact-area radius goes at a slower rate than the reduction of the particle radius, which effectively decreases the area through which heat can conduct using the gas of the macro-gap. As a result of this relative increase of the macro-gap area and decrease of the cavity gap area, $R_G$ will become larger.

Unfortunately no comparison to experimental data is made in literature for the particle diameter, hence it is difficult to remark on the validity of this result on the entire range. However, it was noticed that the mathematical model reaches limits of validity when decreasing the particle size. The model determines the contact area radius, which needs to be smaller than the particle radius for the mathematics to function. For larger particles made or higher Youngs moduli - as with the steel balls initially shown - the contact area radius and the will normally be a few percent of the particle radius. For smaller particles or lower Youngs moduli the contact area radius will increase and can eventually become larger than the particle itself, which the mathematics can not handle.

Quartz sand particles have a contact radius of 20-65% particle radius, which seems quite high and might have a larger error present than the verified steel balls. By own opinion the largest error will most likely be encountered on the lower half of figure **??** and caution should be taken when decreasing the particle diameter even further than shown. Experimental validation of this large contact radius is therefore strongly advised.

A low heat conductivity is preferred in the studied reaction bed to keep the reaction zone narrow. To decrease the heat conductivity it is beneficial to have the following conditions: a decrease of particle size, a decrease of contact force and an increase of the surface roughness. Nevertheless, the influence of the contact force is very small and the surface roughness only shows a large effect at higher values. Additionally both parameters could be more difficult to control in practice if compared to the particle size, which shows a noticeable change to the ETC.

### 4.4.2 Radiation

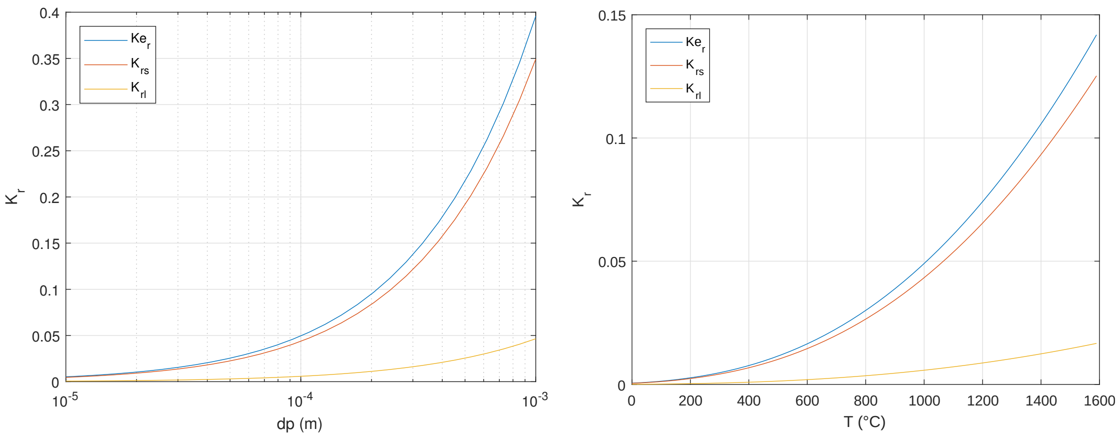


(a) ETC as function of particle diameter at $T = 1500\ K$

(b) ETC as function of temperature with $d_p = 160\mu m$

Figure 4.15: Influence of the particle size and bulk temperature on the ETC due to radiation.

In figure 4.15a is shows that the particle diameter has a significant effect on the ETC. This is apparent by looking at equations (22) and (24) where $k = \mathcal{O}\left(\frac{d_p^3}{d_p^2+C}\right) \approx \mathcal{O}\left(d_p\right)$ which shows an approximate first order behaviour of the ETC as function of the diameter.

Furthermore figure 4.15b looks similar to figure 4.10c so its validity is assumed to be similar; as mentioned in literature it should be accurate up to $1200^o$ C, where after the ETC will be overestimated. Nevertheless the ETC as function of the temperature shows a strong exponential growing influence.

In literature it is mentioned that for radiation to be of importance the particle size and temperature both need to be high [8] [9] [1]. In order to get a better grasp of this a meshplot of both parameters is shown in figure 4.16, which supports this statement. As can be seen, in the region where both the diameter and the temperature are highest the largest ETC is found; if one of the parameters decreases a sharp decline of the ETC is experienced.

In general, to ensure a lower heat conductivity it is beneficial to have the following conditions: a decrease of particle size and a decrease in the bed temperature. The latter is again more difficult to control in practice than the particle size, so for practical applications changing the particle diameter appears to be a promising parameter.

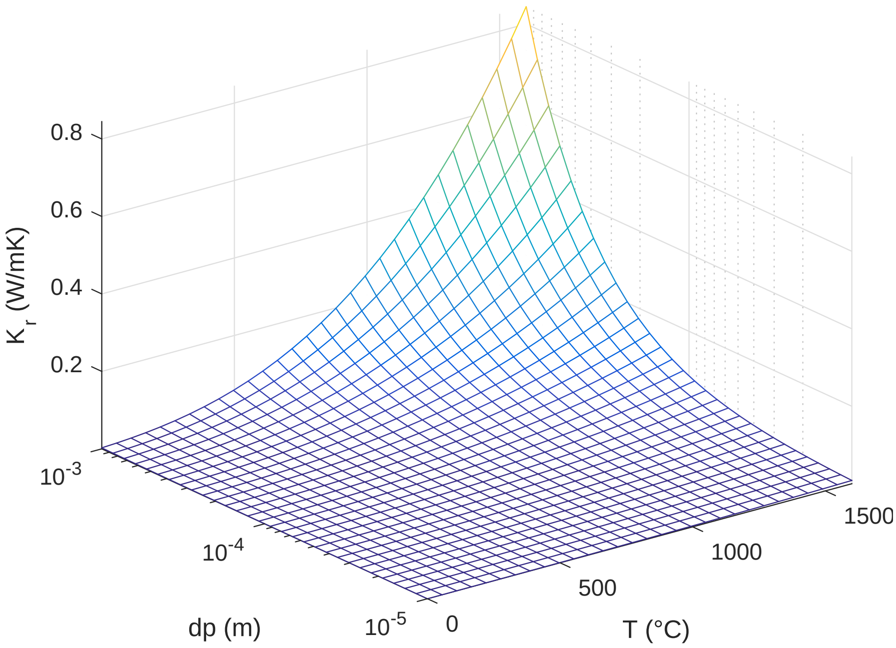


Figure 4.16: Meshed view of the radiation ETC as function of particle diameter and temperature

# 5 FEM model

The mathematical model relies on assumptions and simplifications in order to produce a result. While it has the benefit of producing an analytical result, its application is therefore limited. A FEM model would allow to study cases that can not be determined analytically, like particle size distribution, radiative heat transfer of larger structures, binary beds consisting of different particle types, and can therefore provide better insight in more complex matters.

In order to use result from a FEM model, the numerical simulation should always be validated. Ideally this can be done with experimental results, but in this case it can only be compared with the developed mathematical models, which have been verified in literature to correspond with experimental data. The initial developed FEM model is therefore only verified for analytically known results, for more complex FEM calculations a different method of verification is needed.

A key part of the mathematical model is that is that it incorporates the roughness of the particles, however actually modeling this in FEM would be quite problematic. Looking at how the roughness parameter unfolds itself in the model, it can be seen that it directly influences the size of the contact area and the resistances in the contact area. These results can be used as input for the FEM model, such that the two can be compared with each other.

## 5.1 Conduction

### 5.1.1 Model parts

First a model for conduction was build that would represent the SC unit cell. It consists of two half-spheres of the same diameter which are in contact with each other, while the remaining cavity of the unit cell is separately modeled. The latter is done since convection is not included and it is assumed that the air remain stagnant.

A look can be taken at the half-sphere part in figure 5.1. In the middle of the sphere a separate partition is made for two reasons: the cylindrical partition allows for a structured mesh of the complete half-sphere, and the circular surface at the top now corresponds to the macro-gap from the mathematical model, which can later be used to define contact area between the spheres.

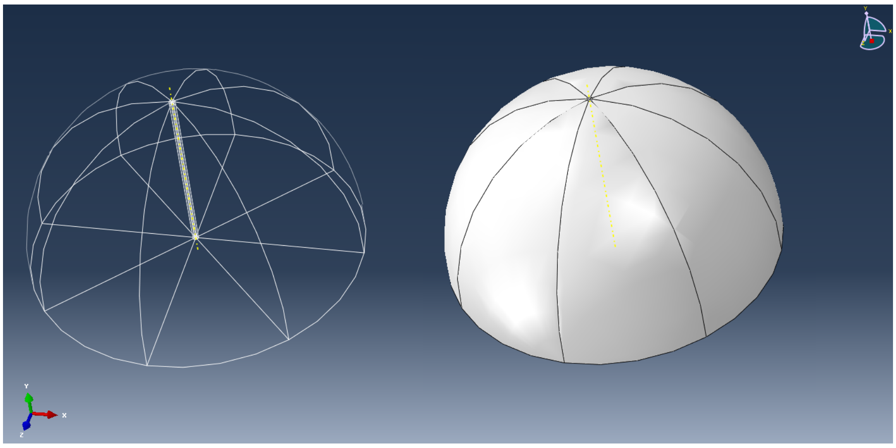

Figure 5.1: Different representations of the half-sphere part.

The surrounding air has the structure as seen in figure 5.2, which only shows half of the cavity. This initial structure proved to be troublesome to decently mesh as a whole, so it has been split up in three separate parts with an easier geometry. The outer layer, the inner layer and a ring in the middle of the cavity. The latter was added to locally increase the mesh density in order to better capture the high heat flux gradient near the contact area. These parts can be seen in figures 5.3a, 5.3b and 5.3c, respectively. Together they can be assembled into the unit cell as shown in figure 5.4.

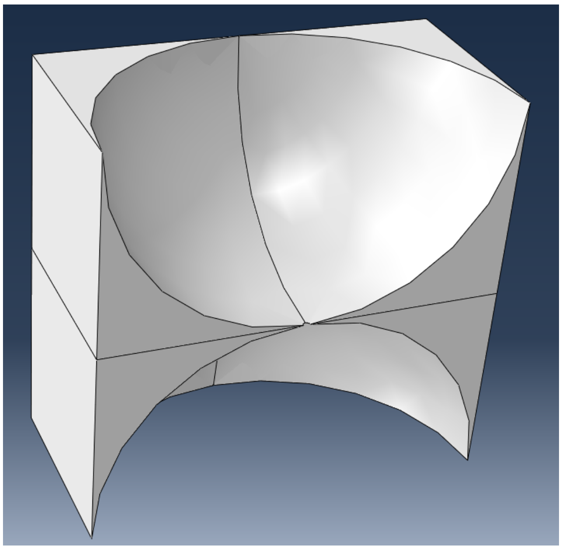

Figure 5.2: Cut-trough of the complete cavity part.

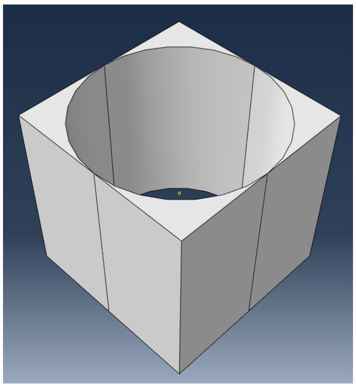

(a) Cavity outer part

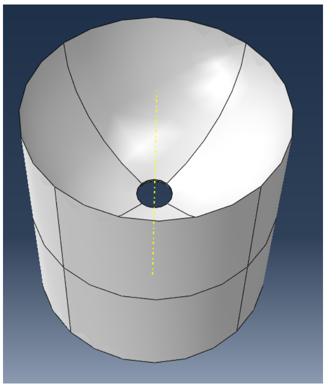

(b) Cavity inner part

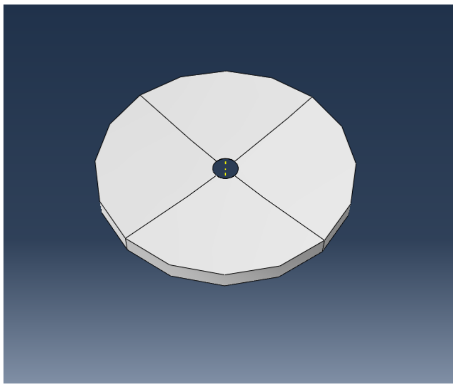

(c) Cavity ring part

Figure 5.3: Separate cavity geometries for easier meshing.

### 5.1.2 Interactions and boundary conditions

For simplicity the actual deformation of the spheres is not modelled. Instead the surfaces on the half-spheres as present in the blue section in figure 5.5 are partitioned, so a surface-to-surface contact interaction can be defined. This interaction contains the contact conductance as function of the gap clearance. This blue section is therefore an empty gap in the model, while in reality it would be pressed against each other. The outer edge of this gap has a certain height, which will increase the resistance. However, due to the short distance compared tot the entire unit cell it could be considered negligible or otherwise be captured in the clearance dependent contact conductance.

The radius of this surface and the contact conductance values are taken from the mathematical model in order to achieve FEM model results that can be compared later on. This approach does have the drawback that the contact problem has to be solved

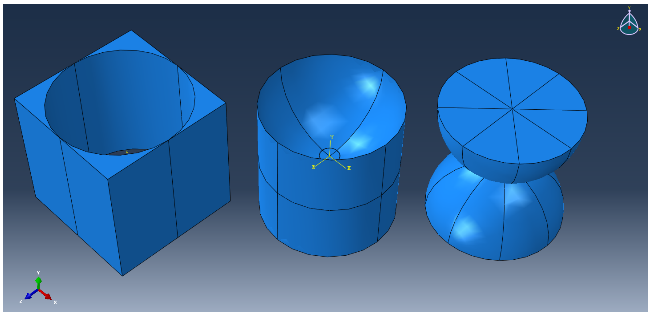

(a) Parts in the assembly module

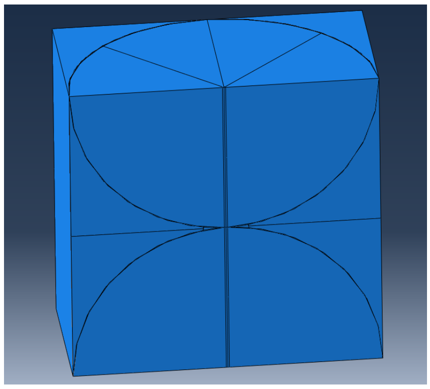

(b) Cut-through of the assembled parts that form the unit cell

Figure 5.4: Parts in the assembly module.

separately before FEM can be used, which is disadvantageous if a more complex case can not be solved analitically. More research on a better contact model is therefore advised.

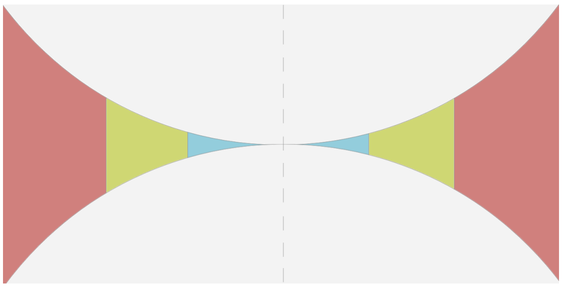

Figure 5.5: Schematic of 2D cut-through showing different zones.

The green section is the ring part where the outer radius is arbitrarily chosen to be ten times the contact area radius, while the red zone is the remainder of the cavity. Furthermore, the contact between the air and the spheres is assumed to be perfect, which is modelled by a tie constraint between the surfaces of both parts. This type of constraint is used to tie two surfaces together during the simulation, which amongst others couples heat transfer on the mesh such that the nodes on a defined slave surface have the same temperature as the master surface. A similar tie is used between the different cavity parts, such that the cavity forms a whole.

The top and bottom of the unit cell are assumed to be isothermal, which is achieved by assigning a temperature BC on both surfaces such to create a $\Delta T$ over the unit cell. The remaining vertical surfaces have no defined BC value, making them automatically behave insulated. This should be, since adjacent unit cells have a parallel temperature gradient to these vertical surfaces, resulting in no heat flux on this boundary.

### 5.1.3 Mesh and quality

The standard element choice of DC3D8 has been chosen for all parts and a structured mesh could be used for the half-sphere, however this was not possible for the cavity. Even after splitting it up in multiple parts with an easier geometry, a structured mesh would create invalid elements due to very large distortions. Instead the following meshing methods where used to get a result: the outer cavity was swept from top to bottom and the inner cavity was swept around the y axis. The entire meshed unit cell can be seen in figure 5.6a.

Since a large heat flux gradient was expected near the contact area it would be beneficial to have a denser mesh around this area, however for both the sphere and the cavity this would also result in invalid elements; this could possibly be a drawback of using this meshing method. Refining the entire part would not be useful, since the greatest heat flux gradients occur only around the contact-point and would become computationally expensive; the ring was added such that the mesh density could be increased locally. This ring could be structurally meshed with a seed bias; this can be seen in figure 5.6b and 5.6c. For the sphere a solution to generate a finer mesh has not been implemented yet, which is something that can be taken into account when optimising the structure.

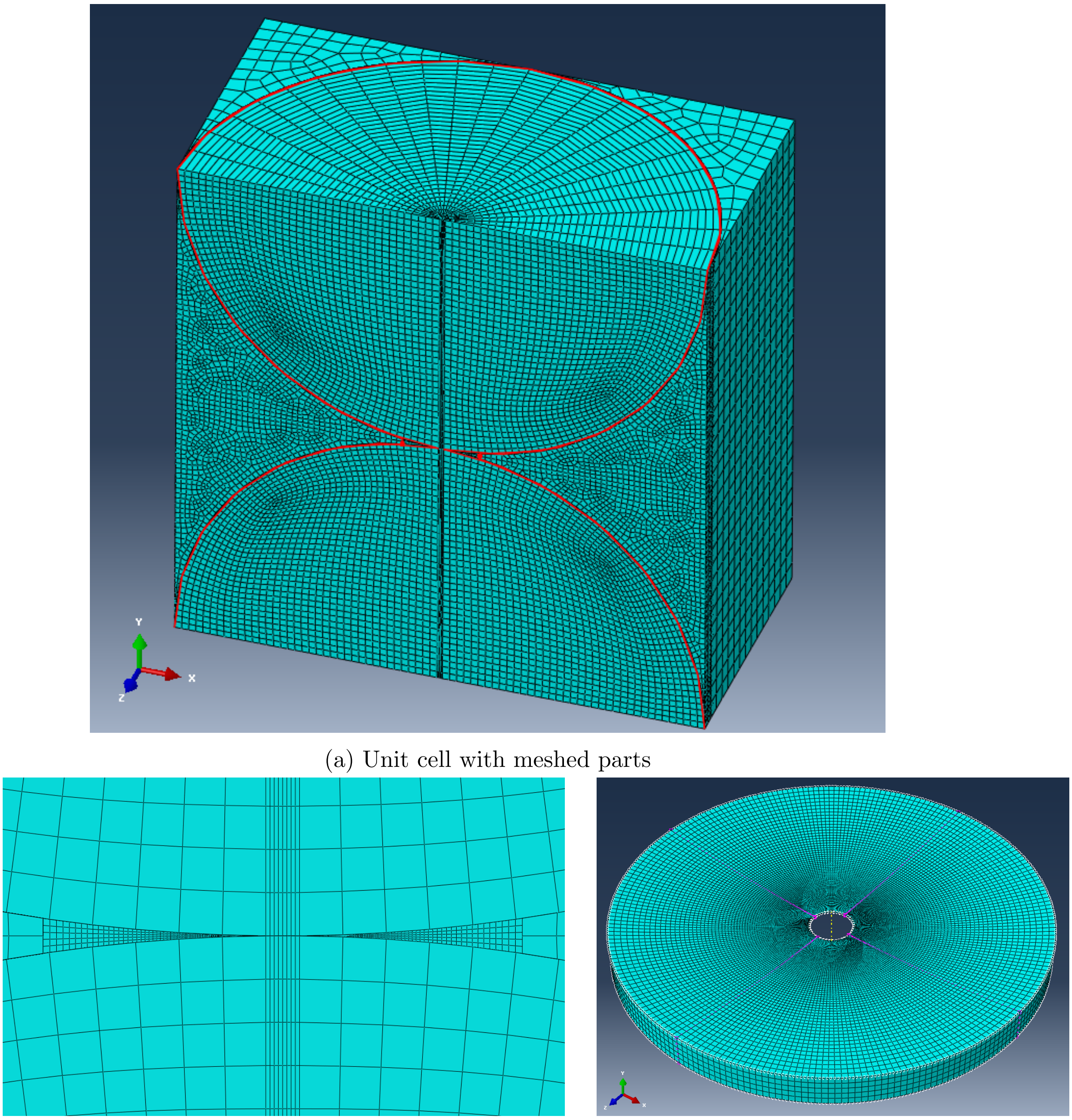

(a) Unit cell with meshed parts

(b) Close up of ring and macro-gap

(c) Biased mesh of the ring

Figure 5.6: Meshed parts of the unit cell.

A look was taken at the numerical results on the mesh for both the temperature and the heat flux. In figure 5.7 the temperature iso-lines can be seen on both the inner cavity and the ring. The iso-lines are supposed to be smooth as seen in the ring, however a numerical error shows as a slight wiggle in the cavity, which means the mesh could be improved upon in future iterations.

The contact-area also shows need of improvement, see figure 5.8. For smaller contact areas the resolution is simply not high enough to properly capture the physics in the spheres, which will create a numerical error. On the other hand it could be argued that this error will have a limited effect on the total heat passing through the unit cell, since the major part will be conducted through the macro-airgap instead of the small contact area. The ring however does seem to give a sufficiently smooth solution, which can be seen in figure 5.9.

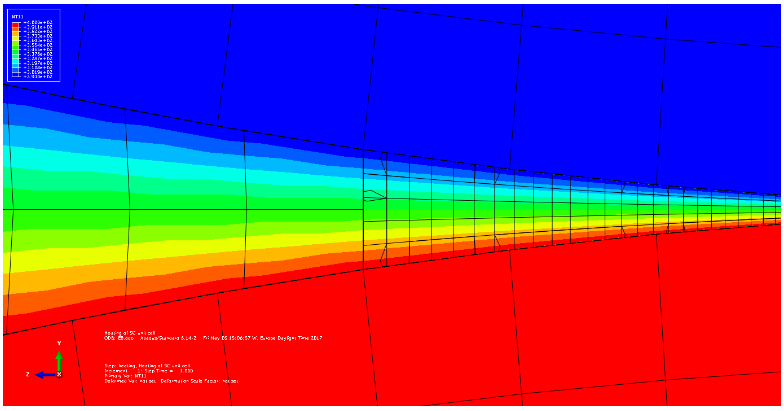

Figure 5.7: Temperature iso-lines inner cavity and ring.

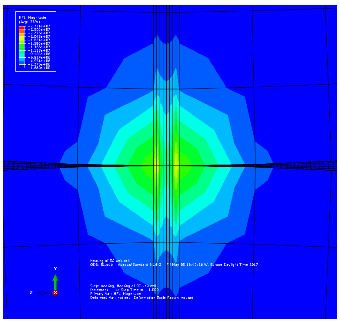

(a) $r_a = 4.0e^{-5}\ m$

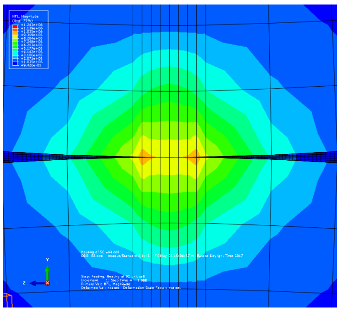

(b) $r_a = 1.4e^{-4}\ m$

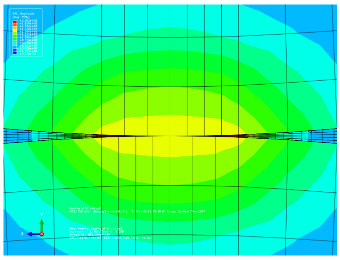

(c) $r_a = 3.5e^{-4}\ m$

Figure 5.8: Heat flux; sphere of fixed diameter $d_p = 1.905e^{-2}\ m$ with changing contact area radius.

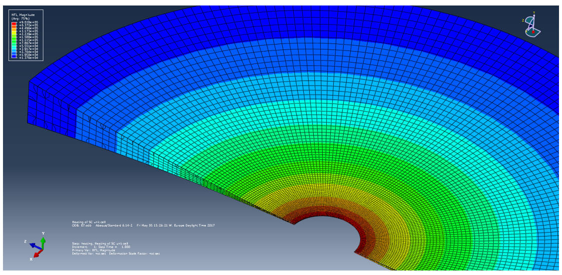

Figure 5.9: Heat flux iso-lines of the ring.

### 5.1.4 Conduction validation

The GUI allows for manual construction of a FEM model, however multiple FEM models had to be created in order to compare them with results from the mathematical model. Changing this manually would be quite vexing. A big advantage of Abaqus is that in the background Python can be used to generate these models, which is very useful in setting specific parameters as variables like the macro-gap radius or the particle radius. In this way an entire model can be generated by means of scripting alone.

One test to validate the conduction model with the mathematical model used several FEM models that had been generated with a different contact area radius. The size of this radius was based on a change in surface roughness from the mathematical model and the thermal contact conductance was determined from the resistances $R_s$ and $R_g$ and the contact area $A_c$ by:

$$H_c = \frac{1}{A_c R_c} \tag{42}$$

where

$$R_c = \left(\frac{1}{R_s} + \frac{1}{R_g}\right)^{-1} \tag{43}$$

For a surface roughness of $\sigma = 2.54\mu m$, the mathematical model gives $H_c \approx 4200$. If compared with values from literature as can be seen in figure 5.10 its value is a bit higher than for stainless steel. The temperature in the model is also higher than the table, which might explain the difference, but nevertheless the mathematical model seems to give a realistic value for thermal conductance.

**TABLE 3–2**

Thermal contact conductance of some metal surfaces in air (from various sources)

| Material | Surface condition | Roughness, μm | Temperature, °C | Pressure, MPa | $h_c$, W/m²·K |
|---|---|---|---|---|---|
| **Identical Metal Pairs** | | | | | |
| 416 Stainless steel | Ground | 2.54 | 90–200 | 0.17–2.5 | 3800 |
| 304 Stainless steel | Ground | 1.14 | 20 | 4–7 | 1900 |
| Aluminum | Ground | 2.54 | 150 | 1.2–2.5 | 11,400 |
| Copper | Ground | 1.27 | 20 | 1.2–20 | 143,000 |
| Copper | Milled | 3.81 | 20 | 1–5 | 55,500 |
| Copper (vacuum) | Milled | 0.25 | 30 | 0.17–7 | 11,400 |

Figure 5.10: Overview of thermal conductances from Çengel's Heat and Mass transfer 4th edition pg. 149.

For every change in roughness a new conductance has been calculated in the same way and could used as input for the FEM model. The used parameters can be seen in table 5.

The total heat going through the lower surface of the unit cell was determined in FEM, which could be used to calculate an effective value for conductivity. The comparison between the mathematical model and the FEM results can be viewed in figure 5.11.

It can be seen that even though the trend is comparable, the result in FEM is much steeper than what the mathematical model predicts and at a roughness of $\sigma = 2.54\mu m$ the value for $k_{eff}$ seems to be underestimated. Since the FEM result is strongly influenced by the input of contact conductance, an explanation for this can be that these values are not correctly calculated. Only one value of conductance at $\sigma = 2.54\mu m$ could be shown to be of an expected magnitude, so it is therefore strongly advised to find a better validation of all values by means of literature, for example.

Table 5: Values from the mathematical model as used in FEM

| **Sphere diameter** $d_p$ $(m)$ | **Particle surface roughness** $\sigma$ $(\mu m)$ | **Contact area radius** $r_a$ $(m)$ | **Conductance** $H_c$ $(W/K)$ |
|---|---|---|---|
| 1.91E-02 | 1.00E-03 | 4.03E-05 | 5.23E6 |
| 1.91E-02 | 2.58E-03 | 4.08E-05 | 3.26E6 |
| 1.91E-02 | 6.64E-03 | 4.22E-05 | 1.96E6 |
| 1.91E-02 | 1.71E-02 | 4.58E-05 | 1.07E6 |
| 1.91E-02 | 4.41E-02 | 5.47E-05 | 4.92E5 |
| 1.91E-02 | 1.14E-01 | 7.24E-05 | 1.86E5 |
| 1.91E-02 | 2.92E-01 | 9.79E-05 | 6.76E4 |
| 1.91E-02 | 7.53E-01 | 1.39E-04 | 2.25E4 |
| 1.91E-02 | 1.94 | 2.15E-04 | 6.57E3 |
| 1.91E-02 | 5.00 | 3.49E-04 | 1.87E3 |

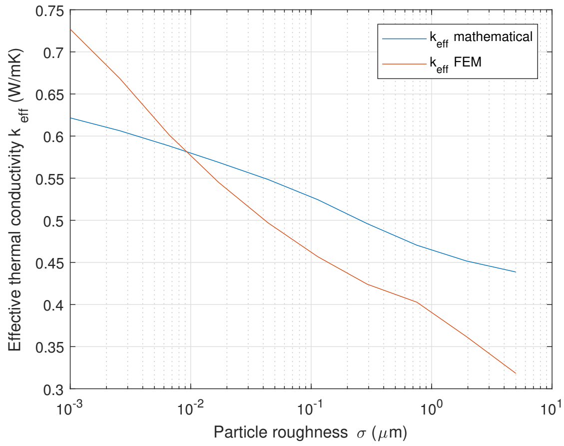


Figure 5.11: Effective thermal conductivity comparison between the mathematical model and the FEM model.

## 5.2 Radiation

### 5.2.1 Model parts

As mentioned in literature the neighbours of the unit cell need to be taken into account to determine the amount of heat transfer by radiation [9]. Radiative calculations quickly become quite time consuming when dealing with many elements, hence thought should be given how to approach this in an efficient way.

The first iteration of this model used the spheres from the conduction model. Initially this made sense, since it would allow for easy unification of both models, however, using multiple of these unit cells became computationally too expensive. The density of the mesh was therefore decreased in order to develop this first take on the model.

Furthermore, a look was taken at the minimal structure that could be simulated. Van Antwerpen considered one complete sphere in the middle, which was surrounded by the bed; symmetry can therefore be used to only model a quarter of the structure. The next issue is the amount of particles that should be simulated. As known from literature, beyond 2.25 particles the radiative contribution to heat transfer tends to zero [9]. The parallel idea in FEM would be that if you have a sole sphere and surround it by one layer of spheres you would notice a different result. Add one additional layer and it will give another difference, but now much less. Finally add a third layer and the result should barely change.

To apply this knowledge, figure 5.12a shows a layer consisting of several adjacent unit cells as seen from the top. In the bottom left corner the 'sole' unit cell can be seen, which is surrounded by additional particles. The red lines have radii of two and two-and-a-half additional spheres in order to visualise which cells should be included. For this model the inner circle was chosen in order to keep the amount of elements as low as possible, resulting in the layer that can be seen in figure 5.12b. These layers were simply stacked on top of each other to account for the remaining particles, creating a quarter cylindrical-like structure. This was done due to simplicity and the way the parts were build, but this will create some unnecessary spheres at the edges. The same optimisation as before could be applied on all axes to create a spherical-like structure, which could perhaps be considered for future iterations. Only layers where stacked on top to save on development time, but layers should also be included at the bottom, such that the red highlighted sphere in figure 5.13 can be investigated.

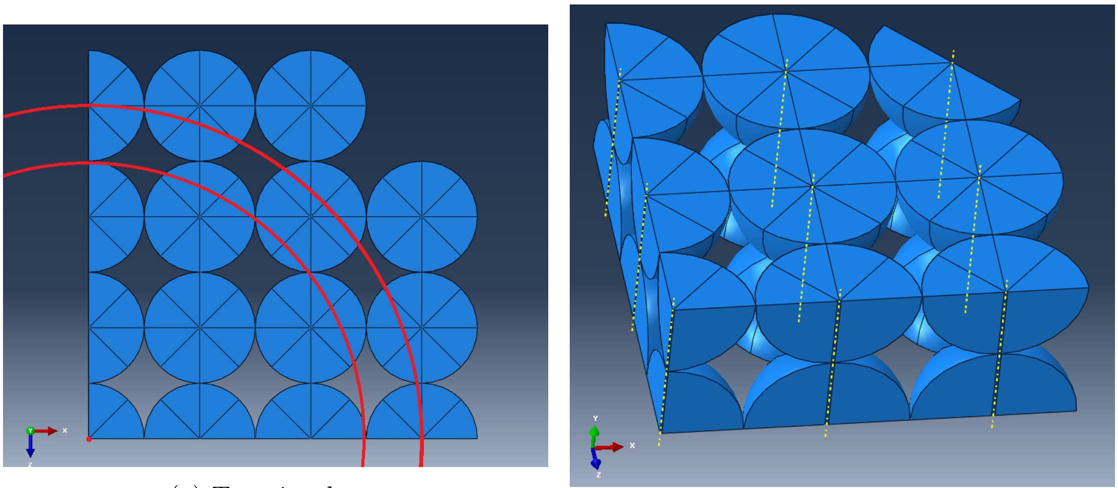

(a) Top view layer

(b) Optimised layer

Figure 5.12: Determining a minimal amount of needed spheres in one layer.

### 5.2.2 Interactions and boundary conditions

A temperature boundary condition is defined on all surfaces at the top and the bottom such to again define a $\Delta T$ of the entire structure. Certain surfaces are set to have no emissivity, such at the top and bottom. This is also the case for the surfaces perpendicular to the X- and Z-axis, since these are used to define a reflective symmetry in order to obtain a simulation representing a fully cylindrical-like structure. Since the spheres originate from the conduction model the partition of the macro-contact area was still present. Seeing that they represent areas that are in contact with each other they have also been assumed to have zero emissivity. The remaining surfaces of the the spheres are then given emissivity properties and a cavity radiation interaction, such that heat transfer by radiation is now possible within the structure.

### 5.2.3 Mesh and validation

As mentioned before, the mesh density has been drastically reduced going from the conduction model to the radiation model, see figure 5.14 for a comparison. The issue of radiative heat transfer computations is that for every element surface a view factor needs to be calculated based on how many other elements surfaces it can 'see', drastically increasing the computation time needed for a finer mesh. Unfortunately, due to shortage

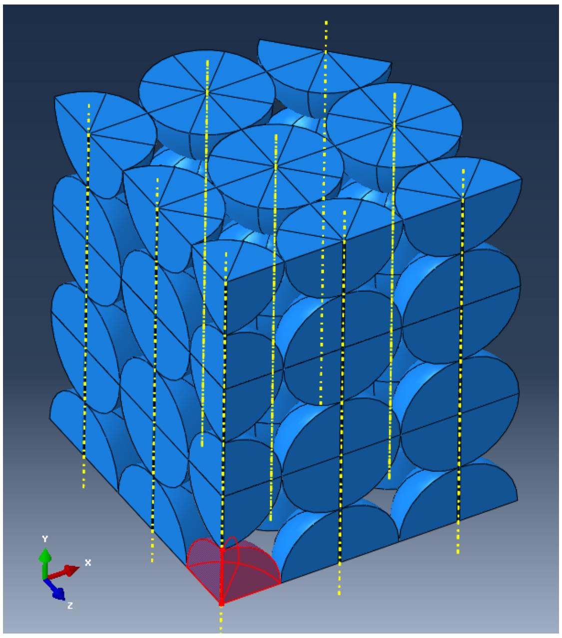

Figure 5.13: A quarter of three layers of stacked particles surrounding the middle sphere highlighted in red.

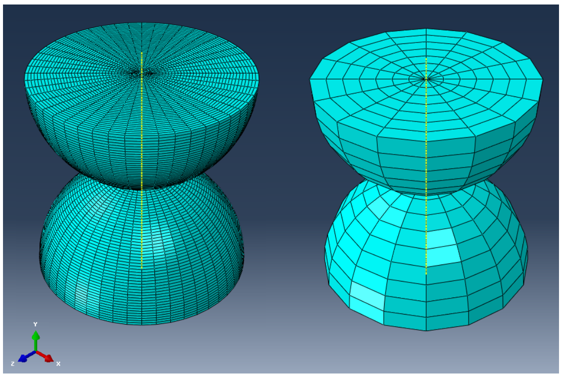

Figure 5.14: Mesh density. Left: conduction sphere. Right: radiation sphere.

in research time it has not been established yet if this mesh is deemed sufficient. It is therefore advised to check for mesh convergence when further developing this radiation model. As a direct result no tests have been run yet to verify the FEM radiation model against data from the mathematical model.

# 6 Discussion

The following points are some remarks on certain aspects of the models.

## 6.1 Bahrami and conduction

The slope correlation was developed based on experimental results of stainless steel and is stated to be accurate up to 15% on other types of metal according to [7]. Due to lack of material data on this specific parameter it was also used for the sand model, but using actual data is preferred.

Furthermore, the model can only accept particles with one given diameter. In reality this diameter will be a distribution of sizes. For now an average size has been taken to determine the mono-bed characteristics of the quartz sand material, but if this assumption can indeed be made should certainly be tested with an experiment.

The beauty of having a single size is that the packed bed can be expressed as a few known standard structures. This allows to homogenize the entire bed by considering the physics on a smaller unit cell level. In the case of binary beds these simple structures can not be made as easily, since they are amongst others influenced by the ratio of the two differently sized particles. Defining all structures for a size-distribution of multiple particles will be unthinkably complex.

Bahrami et al. also researched the effect of different gasses and pressures on the ETC of the bed. Albeit interesting, no attention has been paid to this part of the paper since the process under consideration consists of a bed at standard atmospheric conditions.

When looking at the force as variable parameter: if the particle becomes smaller or roughness increases, for higher values of force the mathematics can produce imaginary results. This has to do with a variable that checks the maximum contact pressure against the material hardness, which if too high will result in negative numbers due to the log function; see equation (64) in the appendix. In the paper nothing is mentioned about this limit of the model, so it should be taken into account.

Lastly, a method to tackle a binary bed consisting of two differently sized particles could be done with the current model. An average size based on the particle distribution of sand and cokes could be taken as the size of two spheres that make up the binary bed. In the case of data provided by ESD the diameter of 1 particle of cokes is approximately 7 time as large as a particle of sand. Taking a SC structure for cokes, this means the sand will be able to fill up the gaps. Normally the properties of air are used to describe these gaps on the cokes-scale, but perhaps sand can be used instead. Imagine that first the model is solved for SC sand, this will give a certain ETC. This value is now used instead of the gas conductivity when solving the model for cokes. Thought should however be given on how to properly approach this and if the final result will indeed correspond to reality.

## 6.2 Van Antwerpen and radiation

As mentioned during the validation it seems that a mistake was made in the radiation model. Only when two variables are interchanged (big N, small n) similar result from literature can be achieved. If however the equations are used as shown a different result is obtained, but according the authors they would have expected said result. Since $n_{long}$ can be chosen in such a way that the overall result matches, this error is of no consequence for the total radiation effective thermal conductivity. It would be wise nevertheless to find validity of especially the magnitude of the short and long radiation components.

The packed bed under research by Van Antwerpen et al. is one of a small annular pebble reactor. Since the walls will have an effect, radial equations are used to correct the porosity for example. Caution should therefore be taken if a small bed is assumed, but for large beds the properties will become the bulk properties again.

As stated in the paper, the deviations observed above 1200C can be attributed to some simplifying assumptions that were made for the the long-range radiation component. First of all, the average temperature difference between a particle under consideration and either a long-range or neighbouring particle is considered to be the same, while in reality this is not the case. Also, the long-range diffuse radiation view factor is a first-order approximation based on an unweighted average value rather than a weighted average for a large number of particles situated at various distances away from the pebble under consideration.

Van Antwerpen et al. also give caution when simulating for lower solid material thermal conductivity values, since the current correlation that are used are only valid for a specific range of $1/\Lambda_s$ values. Additionally the non-isothermal correction factor is assumed to be the same for long and short range radiation, which could be improved to be more accurate at higher temperatures.

Lastly, the paradoxical result with Hertzian contact was shown. In order to get these results the Hertzian contact resistance is used as presented by Van Antwerpen. The origin of the equation can be traced back to the 1973 paper "Conductance of packed spheres in vacuum - Journal of Heat Transfer 95" by Chen & Tien. Unfortunately the paper was unaccessible and therefore it was not possible to properly understand the validity of this resistance and thus the whole contact problem. Gaining deeper knowledge on this contact mechanics is therefore advised.

## 6.3 On both models

A few quick points that are valid for both models. Sometimes parameters like the material conductivity are given a fixed value, while in reality they might be a function of temperature. Implementing this properly could increase the accuracy of both models. At the same time the radiation model accounts for non-isothermal behavior, while the conduction model does not.

In literature the ETC is on multiple accounts defined as the sum of the conduction and radiation components. However, it is never explicitly stated if this assumption is actually true or just that, an assumption. Seeing that how well a particle can conduct influences how well it can radiate intuitively they seem to affect each other. More profound explanations should be found on whether they can indeed and simply be added linearly.

The contact force is taken as an average for the entire bed. While this allows for easier homogenisation, it should be taken into account that in reality the contact load is a function of the height. In reality the temperature field in the bed will be unfluenced by this, which is important since both the materials conductivity and amount of radiation is dependent on temperature.

## 6.4 FEM model

Even though a FEM model was build, the initial developing time was mostly spent on learning the workings of Abaqus. It could therefore contain mistakes that are based on ignorance, therefore a check of the model is advised. Furthermore the model was kept simple in extent in order to validate with analytical results; it should be kept in mind that for more complex FEM calculations a different method of validation is needed.

A first test of verification was made between the conduction model and the mathematical model, but due to lack of time this has not been done for the radiation model. Additionally thought should be put on how to compare them. In the case of conduction the paper had a well defined packed bed, but the paper on radiation contained the measurement of a random bed. Initially three stacked layers had been assembled in FEM, but perhaps layers should be added to the bottom too, such that there will be a particle right in the middle that can be studied.

The amount of needed spheres has only been applied radially in one layer. When stacked this forms a cylinder-like structure, but the same optimization could be performed on all axes, resulting in a sphere-like structure. This will reduce the needed computational time and make for a much more efficient structure.

Actual deformation of the spheres is not included in the model in order to create a simple first version that only accounts for heat transfer. As advantage the contact area and its properties can be defined to be exactly the same as the mathematical model, but a small error will be made due to the larger air gaps around the contact area. Deformation can be included in a next iteration, but the thermal contact resistance which results in the contact conductance property needed for the simulation still needs to be separately solved.

Difficulties were found with using a biased mesh for the cavity and the spheres, since generating a simple mesh was problematic enough to begin with and adding a bias would additionally create many strongly distorted and invalid elements. A finer mesh density was nevertheless needed, but the used GPU was simple not powerful enough to deliver results in the short time available. The ring part of the cavity was therefore added to locally increase the mesh density, but no solution has been implemented yet for the spheres. Either a similar part like the ring can be made for the sphere, or a different method to build and mesh the parts needs to be found, since the results near the contact point show that a finer mesh is most certainly needed.

A practical point for further development is about the contact conductance values. The FEM model relies on these values to be solved separately. This is currently done with the mathematical model, however this approach is disadvantageous if a more complex case can not be solved analytically. More research on an alternative contact model is therefore advised.

As a final note, recent papers by Asakuma et al. [12] [13] [14] show the development of a FEM method solving equations on unit cells level using the same principle of bed homogenisation. This approach could not be taken with the Abaqus, but provides for an interesting read on the subject. Certainly since the authors mention it is a useful tool for modeling heat transfer with radiation in a complex system such as a packed bed.

# 7 Conclusions and recommendations

The research goal was to gain insight in the workings of the heat transfer through a packed bed, by taking into consideration conduction, radiation and the bed properties. From the created models, the following conclusions can be made.

The ETC predicted by the reconstructed model is shown to be a bit overestimated for conduction if compared to literature and the ETC by radiation is definitely too high for temperature higher than 1200 $^oC$. More research should therefore be done to verify the correctness of the magnitudes of the ETC for conduction and radiation, such that the results can be compared with each other. This is useful to determine which of the two is more dominant at a given instance. Nevertheless, the created mathematical models capture the parameters trends as shown in literature very well, which means that the bed behaviour can be predicted and used to gain insight on the characteristics of the packed bed.

Concerning a packed bed using quartz sand properties, the following is noticed. To ensure a lower ETC it is beneficial to have the following conditions for conduction: a decrease of particle size, a decrease of contact force and an increase of the surface roughness. The influence of the contact force is very small over several orders of magnitude and the surface roughness only shows a large effect for values larger than approximately $\sigma = 1\mu m$. The particle size shows a noticeable change to the ETC and could be one of the easiest parameters to modify. For radiation it is beneficial to have the following conditions: a decrease of particle size and a decrease in the bed temperature. The particle diameter might therefore be the easiest parameter to modify and influence the ETC in the bed.

FEM models have been created to complement the analytical mathematical models. The conduction FEM model needs to be revalidated, since the trend matches but the magnitude does not. Furthermore it uses contact solutions from the mathematical model as input, which is disadvantageous if no analytical solution can be found. Thought should be put in how to decouple these two models, such that the FEM model does not have to rely on the mathematical model. The radiation FEM model needs to be further developed as mentioned in the discussion, where after it has to be validated.

# A Appendix A.tex

The number just adjacent of the equations in this appendix point to the location where it is shown in both papers [1] [9], using its equation numbers as reference. Do note that the equations used by Bahrami and Van Antwerpen sometimes slightly differ, and the equations shown here are as Bahrami structured them.

## A.1 Combined material properties

The contact between two Gaussian rough surfaces is modeled by contact between a single Gaussian surface with a combined roughness characteristics of both surfaces and a perfectly smooth surface. The combined roughness $\sigma_{rms}$ and surface slope $m_{rms}$ are:

$$\sigma_{rms} = \sqrt{\sigma_1^2 + \sigma_2^2} \tag{44}$$

$$m_{rms} = \sqrt{m_1^2 + m_2^2} \tag{45}$$

Similarly the conductivity of the materials is combined as:

$$k_s = \frac{2k_1k_2}{k_1 + k_2} \tag{46}$$

The equivalent Vickers micro-hardness is given by:

$$H^{'} = c_1 \left(\frac{\sigma_{rms}}{\sigma_0}\right)^{c_2} \tag{47}$$

In case the Brinell hardness is used, the constants $c_1$ and $c_2$ are found as follows:

$$\begin{aligned} c_1 &= H_{BMG}(4.0 - 5.77\kappa + 4.0\kappa^2 - 0.61\kappa^3) \\ c_2 &= -0.57 + 0.82\kappa - 0.41\kappa^2 + 0.06\kappa^3 \end{aligned} \quad \text{(BA3 VA14)} \tag{48}$$

With the hardness constant $H_{BGM} = 3.178$ GPa, $\kappa = \frac{H_B}{H_{BGM}}$ and $H_b$ is the Brinell hardness of the bulk material. This range is only valid for $1.3 \leq Hb \leq 7.6$ GPa. Else, in case of Vickers microhardness:

$$\begin{aligned} c_1 &= H_{vic} \\ c_2 &= 0 \end{aligned} \quad \text{(BA>3 VA>14)} \tag{49}$$

The equivalent radius of curvature for uniform sized spheres and the effective elastic Young's modulus can be found from:

$$r_{eq} = \frac{r_p}{2} \quad \text{(BA>6 VA>17)} \tag{50}$$

and

$$\frac{1}{E'} = \frac{(1 - \mu_1^2)}{E_1} + \frac{(1 - \mu_2^2)}{E_2} \quad \text{(BA>6 VA>17)} \tag{51}$$

However it was found by Bahrami that using $r_{eq} = r_p$ is more effective and the same approach was taken by Van Antwerpen.

### A.2 Contact area size

The contact area is derived from the maximum contact pressure, after which a correlation is used

$$P_0' = \frac{1}{1 + 1.22\alpha\kappa^{-0.16}} \quad \text{(BA5 VA16)} \tag{52}$$

$$\tag{53}$$

The maximum contact pressure is given by:

$$P_0 = P_0' P_{0,H} \tag{54}$$

where the maximum Hertzian contact pressure is defined as $P_{0,H} = \frac{1.5F}{\pi r_H}$.

The non-dimensional values for $\alpha$ and $\kappa$ are found by:

$$\begin{aligned} \alpha &= \sigma_{rms} \frac{r_p}{r_H^2} \\ \kappa &= \frac{E'}{H_{vic}} \qquad \text{(BA>6 VA>17)} \\ r_H &= \frac{0.75 F r_p}{E'} \end{aligned} \tag{55}$$

Where $r_p$ is the particle diameter, and $r_H$ the Hertzian contact area radius. The rough contact area radius $r_a$ can now be calculated from:

$$r_a = r_c \begin{cases} \frac{1.605}{\sqrt{P_0'}} & 0.01 \leq P_0' \leq 0.47 \\ 3.51 - 2.51 P_0' & 0.47 < P_0' \leq 1 \end{cases} \quad \text{(BA6 VA17)} \tag{56}$$

### A.3 Temperature jump distance

Bahrami et al. states there are four common heat-flow regimes for conduction in gas: continuum, temperature-jump, transition and free-molecular, which are characterized by the Knudsen number. A characteristic distance is given to be:

$$j = \left( \frac{2 - \alpha_{T1}}{\alpha_{T1}} + \frac{2 - \alpha_{T2}}{\alpha_{T2}} \right) \left( \frac{2\gamma_g}{1 + \gamma_g} \right) \frac{\lambda}{Pr} \quad \text{(BA11 VA19)} \tag{57}$$

$\alpha_{T1}$, $\alpha_{T2}$,$\gamma_g$ and Pr serve as thermal coefficients for the surfaces on both particles, where $\gamma_g$ is the gas ratio of specific heats, $Pr$ the Pandtl number and $\lambda$ the molecular mean free-path. A Yovanovich correlation to estimate $\alpha_T$ for engineering surfaces is given to be:

$$\begin{aligned} \alpha_{T,j} = &\exp\left[ -0.57 \left( \frac{T_s - T_0}{T_0} \right) \right] \left( \frac{M^*}{6.8 + M^*} \right) \\ &+ \frac{2.4\mu_g}{(1 + \mu_g^2)} \left\{ 1 - \exp\left[ -0.57 \left( \frac{T_s - T_0}{T_0} \right) \right] \right\} \end{aligned} \quad \text{(BA12 VA20)} \tag{58}$$

Where $M* = M_g$ for mono-atomic gases and $M* = 1.4\ M_g$ for diatomic/polyatomic gases, $T_s$ is the solid surface temperature, $T_0 = 273\ K$ and $\mu_g = \frac{M_g}{M_s}$ the ratio of the molecular masses of the gas and the solid.

## A.4 Thermal joint resistance

With the previous equations it is now possible to calculate the thermal joint resistance $R_j$ with the presence of an interstitial gas:

$$R_j = \left[\frac{1}{\frac{1}{R_s} + \frac{1}{R_g} + R_L} + \frac{1}{R_G}\right]^{-1} \quad \text{(BA1)} \tag{59}$$

It contains the following four thermal resistance components. The first is the thermal constriction/spreading resistance $R_s$ through the micro-contacts and assumes plastically deformed asperities:

$$R_s = \frac{0.565}{k_s F} \frac{\sigma_{rms}}{m_{rms}} \quad \text{(BA2 VA13)} \tag{60}$$

The constriction/spreading resistance is given by:

$$R_L = \frac{0.5}{k_s r_a} \quad \text{(BA8 VA18)} \tag{61}$$

The non-conforming region between the solids was divided into infinitesimal surface elements, which were integrating in order to find an expression for the thermal resistances of the microgap and the macrogap:

$$R_g = \frac{2\sqrt{2}\sigma_{rms} a_2}{\pi k_g r_a^2 \ln\left(1 + \frac{a_2}{a_1 + \frac{M}{2\sqrt{2}\sigma_{rms}}}\right)} \quad \text{(BA13 VA21)} \tag{62}$$

$$R_G = \frac{2}{\pi k_g \left[S \ln\left(\frac{S-B}{S-A} + B - A\right)\right]} \quad \text{(BA14 VA28)} \tag{63}$$

where

$$\begin{aligned} a_1 &= erfc^{-1}\left(\frac{2P_0}{H'}\right) \\ a_2 &= erfc^{-1}\left(\frac{0.03P_0}{H'}\right) - a_1 \end{aligned} \quad \text{(BA13)} \tag{64}$$

$$\begin{aligned} A &= 2\sqrt{r_p^2 - r_a^2} \\ B &= 2\sqrt{r_p^2 - b_l^2} \\ S &= 2(r_p - \omega_0) + j \\ \omega_0 &= \frac{r_a^2}{2r_p} \end{aligned} \quad \text{(BA14)} \tag{65}$$

Here the macrogap chord $b_L = r_p$ and $\omega_0$ is the depth of deformation in m.

## References

[1] Majid Bahrami, M. Michael Yovanovich, and J. Richard Culham. Effective thermal conductivity of rough spherical packed beds. *International Journal of Heat and Mass Transfer*, 49(19-20):3691–3701, 2006.

[2] Hao Wu, Nan Gui, Xingtuan Yang, Jiyuan Tu, and Shengyao Jiang. Effect of scale on the modeling of radiation heat transfer in packed pebble beds. *International Journal of Heat and Mass Transfer*, 101:562–569, 2016.

[3] Alan J. Slavin, Frank A. Londry, and Joy Harrison. A new model for the effective thermal conductivity of packed beds of solid spheroids: alumina in helium between 100 and 500C. *International Journal of Heat and Mass Transfer*, 43(12):2059–2073, 2000.

[4] Alan J. Slavin. Test of a new model for the temperature and pressure dependence of the thermal conductivity of a packed pebble bed in gas: lithium zirconate in helium. *Fusion Engineering and Design*, 54(1):87–95, 2001.

[5] A.J. Slavin, E. Irvine, and S. Penson. Analytical model for the thermal conductivity of a binary bed of packed spheroids in the presence of a static gas, with no adjustable parameters provided contact conductance is negligible. *International Journal of Heat and Mass Transfer*, 47(5):1015–1021, 2004.

[6] M. Bahrami, M. M. Yovanovich, and J. R. Culham. Thermal Joint Resistances of Nonconforming Rough Surfaces with Gas-Filled Gaps. *Journal of Thermophysics and Heat Transfer*, 18(3):326–332, 2004.

[7] M Bahrami, J R Culham, and M M Yovanovich. Modeling thermal contact resistance: A scale analysis approach. *J. Heat Transfer*, 126(6):896–905, 2004.

[8] W. van Antwerpen, C.G. du Toit, and P.G. Rousseau. A review of correlations to model the packing structure and effective thermal conductivity in packed beds of mono-sized spherical particles. *Nuclear Engineering and Design*, 240(7):1803–1818, 2010.

[9] W. Van Antwerpen, P. G. Rousseau, and C. G. Du Toit. Multi-sphere Unit Cell model to calculate the effective thermal conductivity in packed pebble beds of mono-sized spheres. *Nuclear Engineering and Design*, 247:183–201, 2012.

[10] Xiaoliang Wang, Jie Zheng, and Hongli Chen. A prediction model for the effective thermal conductivity of mono-sized pebble beds. *Fusion Engineering and Design*, 103:136–151, feb 2016.

[11] Xiaoliang Wang, Jie Zheng, and Hongli Chen. Application of a model to investigate the effective thermal conductivity of randomly packed fusion pebble beds. *Fusion Engineering and Design*, 106:40–50, may 2016.

[12] Yusuke Asakuma and Tsuyoshi Yamamoto. Effective Thermal Conductivity with Convection and Radiation in Packed Bed. *Journal of Energy and Power Engineering*, 7:639–646, 2013.

[13] Yusuke Asakuma, Yushin Kanazawa, and Tsuyoshi Yamamoto. Thermal radiation analysis of packed bed by a homogenization method. *International Journal of Heat and Mass Transfer*, 73:97–102, 2014.

[14] Yusuke Asakuma, Masahiro Asada, Yushin Kanazawa, and Tsuyoshi Yamamoto. Thermal analysis with contact resistance of packed bed by a homogenization method. *Powder Technology*, 291:46–51, 2016.